JEM

Article

Iron modulation of erythropoiesis is associated with Scribble-mediated control of the erythropoietin receptor

Shadi Khalil,[1]* Lorrie Delehanty,[1]* Stephen Grado,[1] Maja Holy,[1] Zollie White III,[1] Katie Freeman,[1] Ryo Kurita,[2,3] Yukio Nakamura,[2,3] Grant Bullock,[4] and Adam Goldfarb[1]

[1]Department of Pathology, University of Virginia School of Medicine, Charlottesville, VA
[2]Cell Engineering Division, RIKEN BioResource Center, Tsukuba, Ibaraki, Japan
[3]Comprehensive Human Sciences, University of Tsukuba, Tsukuba, Ibaraki, Japan
[4]Department of Pathology, University of Pittsburgh Medical Center, Pittsburgh, PA

Iron-restricted human anemias are associated with the acquisition of marrow resistance to the hematopoietic cytokine erythropoietin (Epo). Regulation of Epo responsiveness by iron availability serves as the basis for intravenous iron therapy in anemias of chronic disease. Epo engagement of its receptor normally promotes survival, proliferation, and differentiation of erythroid progenitors. However, Epo resistance caused by iron restriction selectively impairs proliferation and differentiation while preserving viability. Our results reveal that iron restriction limits surface display of Epo receptor in primary progenitors and that mice with enforced surface retention of the receptor fail to develop anemia with iron deprivation. A mechanistic pathway is identified in which erythroid iron restriction down-regulates a receptor control element, Scribble, through the mediation of the iron-sensing transferrin receptor 2. Scribble deficiency reduces surface expression of Epo receptor but selectively retains survival signaling via Akt. This mechanism integrates nutrient sensing with receptor function to permit modulation of progenitor expansion without compromising survival.

INTRODUCTION

Erythropoiesis, the process of RBC production, claims ∼80% of the iron flux in mammals (Ganz and Nemeth, 2012). When iron delivery falls below a critical threshold, erythroid progenitors promptly enact a lineage-specific response suppressing proliferation and differentiation while retaining viability (Kimura et al., 1986; Rozman et al., 1992; Choi, 2007; Bullock et al., 2010; Camaschella, 2015; Nai et al., 2015; Zhao et al., 2016). This response preserves limited iron stores for vital functions but also underlies the pathogenesis of iron-restricted anemias: iron deficiency anemia (IDA) and anemia of chronic disease and inflammation.

The principal pathogenetic mechanism in iron-restricted anemias involves development of marrow resistance to the cytokine erythropoietin (Epo). Epo normally acts on early hematopoietic progenitors to promote erythroid lineage commitment and on erythroblasts to mediate survival, proliferation, and differentiation (Lodish et al., 2010; Grover et al., 2014; Aljitawi et al., 2016). Patients with IDA strongly increase serum Epo levels, with responses actually exceeding those of iron-replete subjects matched for hypoxia (Frise et al., 2016). However, their marrows fail to undergo compensatory hyperplasia and contain the same number of erythroblasts as marrows from iron-replete subjects (Choi, 2007). Furthermore, patient responses to exogenous Epo in anemia of chronic kidney disease critically depend on iron availability (Drüeke, 2001; Elliott et al., 2009). Thus, intravenous iron is often administered to abrogate clinical Epo resistance (Sunder-Plassmann and Hörl, 1995, 1997; Rosati et al., 2015).

How iron deprivation mechanistically alters the erythroblastic response to Epo remains unresolved but appears to involve a specialized mechanism. Responsiveness to all cytokines is not impaired, and inflammatory mediators such as TNF-α and IFN-γ actually exert magnified rather than blunted effects on iron-deprived erythroblasts (Richardson et al., 2013). In addition, iron deficiency does not uniformly restrict all features of the Epo response but rather restrains proliferation and differentiation while preserving prosurvival signaling (Tanno et al., 2008; Bullock et al., 2010; Nai et al., 2015; Zhao et al., 2016). Iron-sensing molecules implicated in erythropoietic regulation include aconitase enzymes and transferrin receptors. Aconitase conversion of citrate to isocitrate uses an active site $4Fe^{2+}$-4S cluster, which is highly sensitive to iron restriction in the erythroid lineage (Bullock et al., 2010). A functional role for aconitase is suggested by the reversal of the erythroid iron deprivation response with isocitrate treatment and by selective inhibition of erythropoiesis with a targeted enzyme inhibitor (Bullock et al., 2010; Talbot et al., 2011; Richardson et al., 2013; Gunawardena et al., 2016; Kim et al., 2016). The erythroid- and liver-specific transferrin receptor 2 (TfR2) also responds to iron depri-

*S. Khalil and L. Delehanty contributed equally to this paper.

Correspondence to Adam Goldfarb: ang3x@virginia.edu

The Rockefeller University Press
J. Exp. Med. 2018 Vol. 215 No. 2 661–679
https://doi.org/10.1084/jem.20170396

vation, shifting from recycling to lysosomal catabolism in response to decreases in its ligand holotransferrin (Johnson and Enns, 2004; Johnson et al., 2007). Its contribution to the erythroid iron deprivation response has been demonstrated by the inappropriate erythroblastic expansion observed in iron-deficient mice with erythroid TfR2 knockout (Nai et al., 2015; Rishi et al., 2016).

This study delineates a molecular pathway by which iron availability dictates the Epo response in erythroid progenitors. Direct involvement of the Epo receptor (EpoR) is demonstrated by its impaired surface presentation caused by iron deprivation and by the loss of the iron deprivation response in mice with a receptor mutation causing surface trapping. Scribble, a master regulator of receptor trafficking and signaling, is identified as a novel iron response factor that coordinates EpoR surface levels and amplitude of Akt signaling. Specifically, erythroid iron deprivation caused Scribble down-regulation through a cathepsin- and TfR2-dependent mechanism. Scribble deficiency in turn compromised EpoR surface delivery while enhancing Akt activation, thus providing a means for integration of iron sensing with Epo responsiveness.

RESULTS

EpoR surface modulation is a critical component of the erythroid iron deprivation response

Because Epo resistance is a critical feature of the erythroid iron deprivation response, we examined whether EpoR is affected by this pathway. To this end, primary human erythroid progenitors were subjected to overnight iron withdrawal or enzymatic aconitase inhibition followed by surface biotinylation, streptavidin pull-down, and immunoblot. We have previously shown in these progenitors that aconitase inhibition with 50 μM sodium fluoroacetate (FA) recapitulates the iron deprivation phenotype and does not impair viability (Talbot et al., 2011). With these overnight treatments, total membrane-associated EpoR levels remained unaffected (Fig. 1 B). In contrast, surface EpoR levels underwent major decreases (approximately threefold) with both treatments, whereas overall levels of surface-biotinylated proteins remained unaffected (Fig. 1 A). By the same approach, iron withdrawal had no significant effect on surface levels of TfR1 (Fig. S1 A). To determine whether this receptor modulation affected capacity for downstream signaling, iron-replete and -deprived progenitors underwent cytokine starvation followed by Epo stimulation for 0, 10, and 30 min. Consistent with their diminished surface EpoR levels, iron-deprived progenitors showed an approximately threefold decrease in peak phosphorylation of STAT5 at 10 min (Fig. 1 C).

To assess whether alterations in EpoR surface expression contribute to the erythroid iron deprivation response, we analyzed mice with the *EpoR-H* knock-in mutation. This mutant allele causes truncation of the distal cytoplasmic domain containing motifs essential for receptor internalization (Sulahian et al., 2009) but retains the tyrosine 434 residue critical for productive JAK2 signaling (Menon et al., 2006). Thus, EpoR-H signals normally in response to Epo, but fails to execute the subsequent internalization and degradation characteristic of WT EpoR (Becker et al., 2010). Under normal conditions, adult *EpoR-H* mice displayed no evidence of splenic stress erythropoiesis (not depicted) and had a subtle but significant shift toward immaturity in marrow erythroid progenitors (Fig. S1 B). Their steady-state serum Epo levels were diminished approximately threefold compared with WT animals, consistent with enhanced progenitor sensitivity (Fig. S1 C). For assessment of in vivo iron deprivation responses, WT and *EpoR-H* mice were placed on an iron-deficient diet and monitored weekly for blood cell counts and indices. At the start of the study, the *EpoR-H* mice had elevated RBC numbers but normal size mean corpuscular volume. After several weeks of iron deprivation, WT animals manifested an RBC decline, which was highly significant at 42 d. In contrast, the iron-deprived *EpoR-H* animals displayed no decline in RBC throughout the entire period (Fig. 1 D). Notably, both strains developed significant microcytosis over this period, with similar magnitudes and kinetics. Under conditions of iron deprivation, no discernable differences in marrow erythroid maturation were seen between strains (not depicted); however, a trend toward increased splenic erythroid maturation was observed in *EpoR-H* mice (Fig. S1 D).

To compare ex vivo iron deprivation responses, we isolated Lin^- Kit^+ $Ter119^-$ erythroid stress progenitors from spleens of hemolytically challenged WT and *EpoR-H* mice. These progenitors were then subjected to culture in a defined system adapted from iron deprivation studies in human progenitors (Bullock et al., 2010). Specifically, this system used serum-free medium with specified TSATs and included an isocitrate treatment, which is known to reverse the erythroid iron deprivation response (Bullock et al., 2010). With mouse progenitors, these culture conditions permitted an assessment of early erythroid differentiation, marked by CD71 up-regulation, and provided an iron deprivation response reversible by isocitrate (Fig. 1 E). Notably, progenitors from the *EpoR-H* mice showed a complete loss of responsiveness to iron deprivation and isocitrate (Fig. 1, E and F), consistent with a cell-intrinsic role for surface EpoR modulation.

Scribble is regulated by the erythroid iron deprivation response and influences surface EpoR display

The alterations in surface EpoR seen with iron deprivation suggested the potential involvement of Scribble, a large multidomain regulator of receptor trafficking and signaling (Lahuna et al., 2005; Michaelis et al., 2013; Piguel et al., 2014). Notably, several features of the erythroid iron deprivation response phenocopy changes reported with deficiency of Scribble: hyperactivation of multiple kinase pathways (Bullock et al., 2010; Nagasaka et al., 2010, 2013; Li et al., 2011; Elsum et al., 2013), enhanced formation of endocytic vesicles (Rozman et al., 1992; Igaki et al., 2009), and sensitization of cells to TNF-α (Igaki et al., 2009; Richardson et

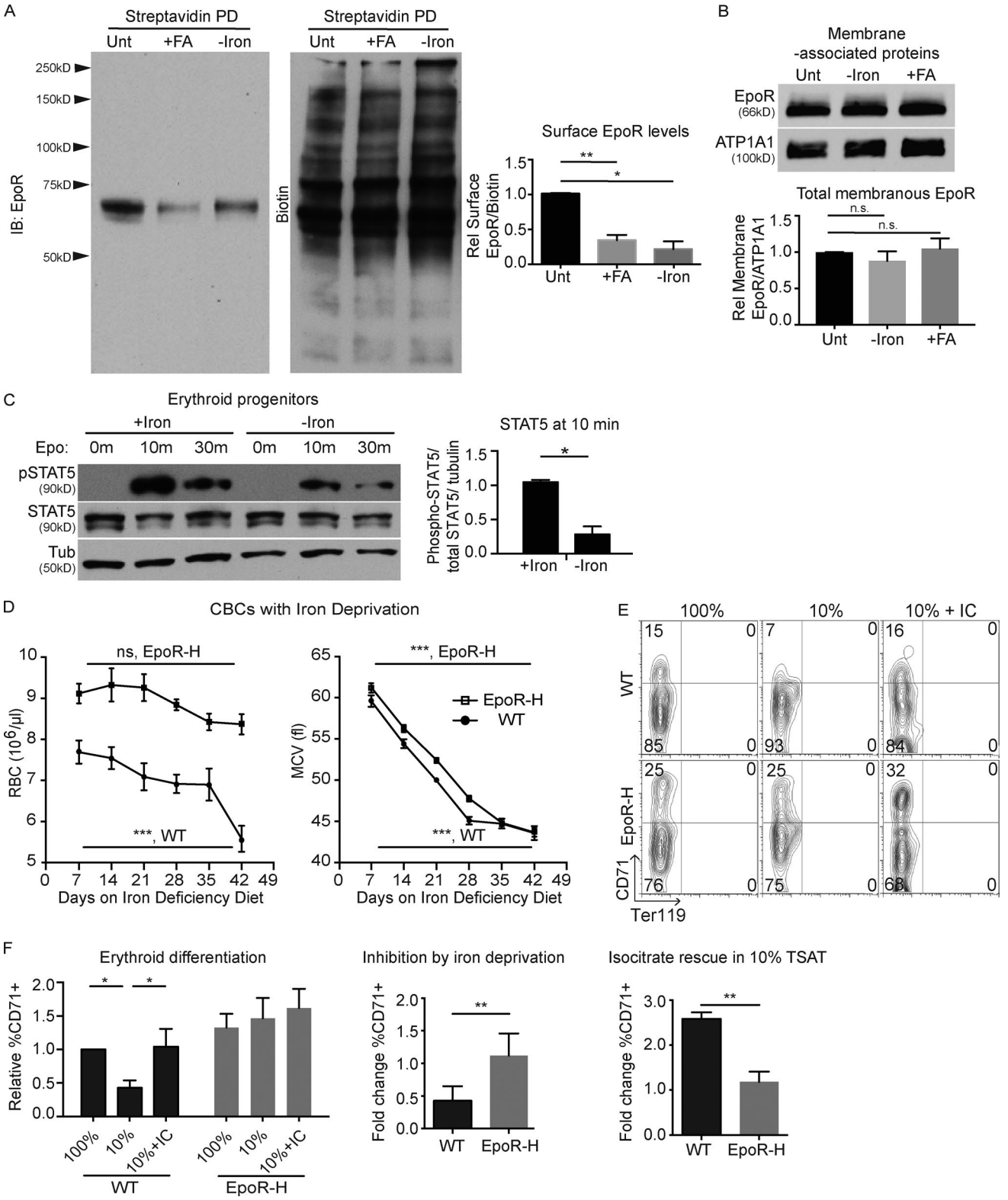

Figure 1. **EpoR surface modulation is a critical component of the erythroid iron deprivation response. (A)** Immunoblots of surface-biotinylated proteins from erythroid progenitors untreated or subjected to 16 h of iron deprivation or FA treatment and densitometry from multiple experiments for relative levels of surface EpoR associated with treatments, with normalization to total biotinylated protein levels ($n = 4$, one-way ANOVA; IB, immunoblot; PD, pull-down). **(B)** Immunoblots of total membrane fractions from erythroid progenitors, untreated or subjected to 16 h of iron deprivation or 50 µM

al., 2013). Furthermore, within the hematopoietic hierarchy in humans and mice, *SCRIB* expression demonstrated lineage- and stage-selective modulation in erythroid progenitors (Bagger et al., 2016). Specifically *SCRIB* underwent dramatic up-regulation at the first committed erythroid stage, corresponding to BFU-E, followed by down-regulation in subsequent stages (Fig. 2 A and Fig. S2 A).

Immunoblot analysis of human erythroblasts identified Scribble in cytosolic and membrane fractions as three to four species ranging from ∼180 to 250 kD, with the largest form predominating in the cytosolic and whole cell lysate preparations (Fig. 2 B). Assay specificity was confirmed using multiple independent antibodies and shRNA knockdown (Fig. S2, B and C). The basis for the multiple species appeared to arise, at least in part, from differential ubiquitylation, as treatment of cells with a deubiquitylase inhibitor induced a pattern shift to predominance of the largest form (Fig. S2 D). Importantly, Scribble levels in both fractions underwent robust down-regulation with erythroid iron deprivation and showed restoration with isocitrate treatment (Fig. 2 B). Immunofluorescence on iron-replete erythroblasts revealed Scribble to be concentrated at the periphery of the cell, but also distributed throughout the cytoplasm in a vesicular pattern (Fig. 2 C). Scribble displayed a pancellular decrease with iron deprivation, and isocitrate treatment rescued expression particularly at the cell periphery (Fig. 2 C). In contrast to the protein changes, *SCRIB* transcripts did not decline with iron deprivation and did not respond to isocitrate (Fig. 2 D). To address the basis for Scribble down-regulation at the protein level, iron-deprived erythroblasts were screened with a series of protease inhibitors. As shown in Fig. 2 E, treatment of cells with a cell-permeable cathepsin inhibitor CA074me prevented Scribble down-regulation by iron deprivation (Fig. S2 E). In iron-replete cells, cathepsin inhibition minimally affected cytosolic Scribble but did increase membrane levels.

To determine the consequences of Scribble down-regulation on EpoR trafficking, primary progenitors underwent lentiviral shRNA-mediated knockdown. As shown in Fig. 2 F, Scribble knockdown in these cells markedly diminished surface EpoR expression, but concomitant decrease in total EpoR levels (likely caused by impaired maturation as shown in Fig. 3 C and Fig. S3 B) complicated the interpretation of these findings. To circumvent this limitation, we also knocked down Scribble in HUDEP-2 cells, a nontransformed human erythroblast cell line (Kurita et al., 2013). In these cells, Scribble knockdown strongly decreased surface EpoR while minimally affecting total cellular levels (Fig. 2 G).

Scribble regulates erythropoiesis, and its deficiency phenocopies characteristics of the erythroid iron deprivation response

Previous ultrastructural comparisons of erythroblasts from iron-deficient and -replete human marrow samples revealed a highly significant ($P < 0.001$) increase in empty cytoplasmic vesicles associated with iron deficiency (Rozman et al., 1992). This finding correlates with the erythrocyte vesicles specifically found in peripheral blood smears of iron-deficient subjects (Harrington et al., 2008). We therefore determined whether deficiency of Scribble, known to regulate vesicle formation in *Drosophila melanogaster* (Igaki et al., 2009), affected erythroid ultrastructure. In these studies, electron microscopy (EM) of erythroid progenitors demonstrated an association of Scribble deficiency with increases in peripheral empty vesicles, resembling those that Rozman et al. (1992) identified in patients with IDA (Fig. 3, A and B). Cells deficient in Scribble also displayed increases in larger vesicles with intraluminal vesicle formation.

Prior studies have determined that iron restriction of human progenitors cultured in unilineage erythroid medium for 3–5 d impairs their up-regulation of surface glycophorin A (GPA) on flow cytometry (Bullock et al., 2010; Richardson et al., 2013). Therefore, we used this assay system to assess the consequences of Scribble deficiency under iron-replete conditions. Strikingly, knockdown of Scribble blocked GPA up-regulation in day 4 erythroid cultures while fully maintaining cell viability (Fig. 3, C and D; and Fig. S3 A). As previously described for iron restriction (Richardson et al., 2013), this blockade preferentially affected the later erythroid marker GPA while permitting up-regulation of the earlier marker CD36 (Fig. S3 B). To assess the role of Scribble in mouse erythropoiesis, *Scrib* floxed (f) animals were mated with a variety of deleter strains. Poor deletion efficiency was obtained with the *EpoR-Cre* and *Vav-Cre* strains. An additional problem with *EpoR-Cre* is that *EpoR* up-regulation lags behind that of *Scrib* during erythroid development. Our studies therefore focused on animals with germline excision

FA treatment and densitometry from multiple experiments for relative levels of EpoR associated with treatments, with normalization to ATP1A1 ($n = 3$, one-way ANOVA). **(C)** Immunoblot analysis of iron-replete and -deprived erythroid progenitors subjected to cytokine starvation and Epo stimulation for 0, 10, and 30 min and densitometry from multiple experiments for fold change in STAT5a/b phosphorylation at 10 min associated with iron deprivation ($n = 3$, two-way ANOVA). Unt, untreated; +FA, FA treated; −Iron, iron deprived; +Iron, iron-replete. **(D)** Circulating RBC count and RBC mean corpuscular volume (MCV) values in WT and *EpoR-H* mutant mice subjected to dietary iron deprivation for the indicated number of days ($n = 12$ per group, intragroup comparisons between day 7 and day 42 values, repeated measures two-way ANOVA; CBC, complete blood count). **(E)** Flow cytometry of splenic Lin^- Kit^+ progenitors from WT and *EpoR-H* mutant mice cultured in erythroid medium with transferrin saturations (TSATs) of 100% or 10% ± isocitrate. **(F)** Summary of multiple flow cytometry studies as in E, showing fold change in the percentage of $CD71^+$ cells normalized to WT progenitors cultured in medium with 100% TSAT, fold change in the $CD71^+$ percentage associated with iron deprivation, and fold increase in the $CD71^+$ percentage associated with isocitrate treatment of iron-deprived cells (right; $n = 3$; left: two-way ANOVA; middle and right: Student's t test). Graphs depict mean ± SEM from the indicated number of independent experiments. *, $P < 0.05$; **, $P < 0.01$; ***, $P < 0.001$. IC, isocitrate; ns, not significant.

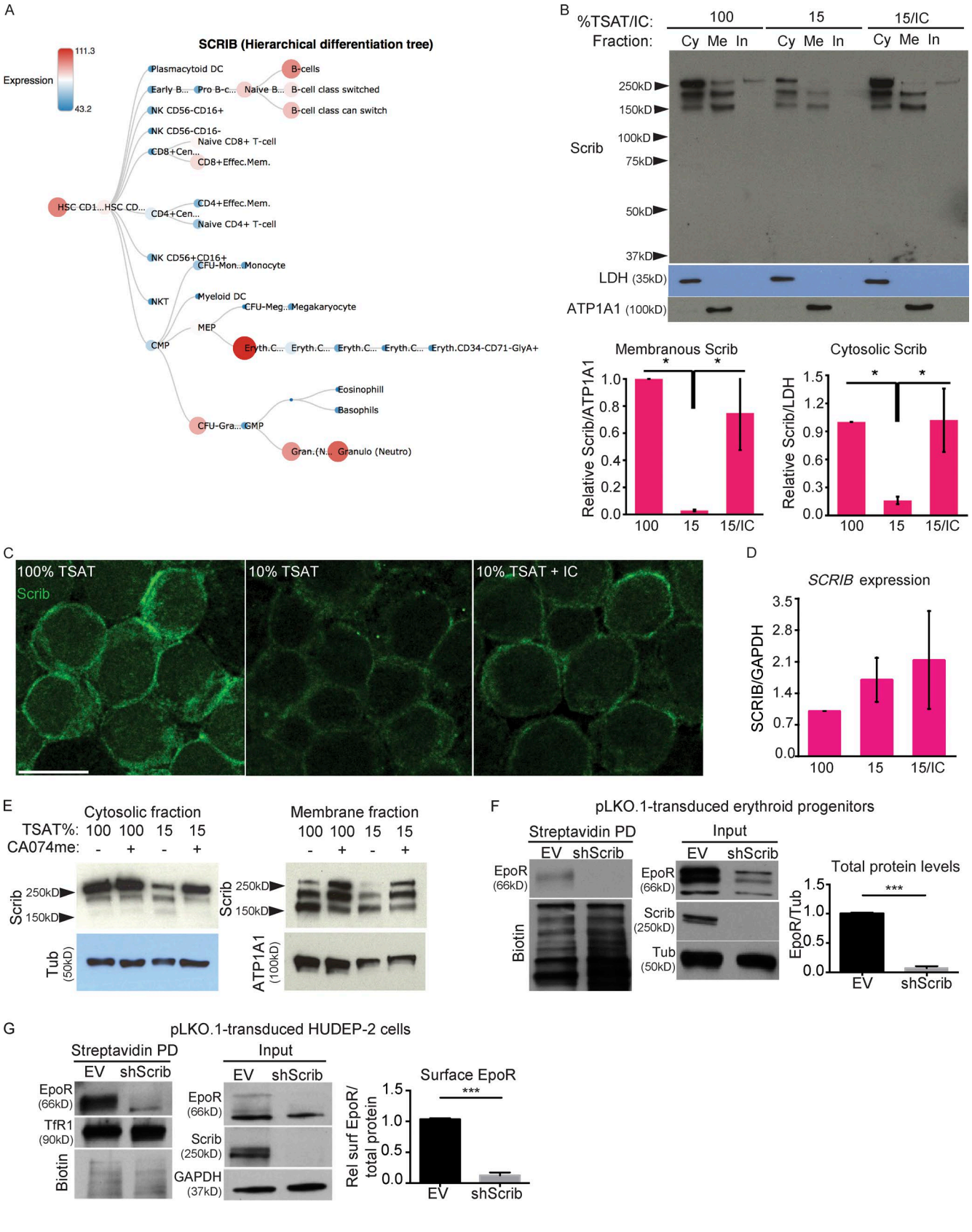

(Δ). Because of the neonatal (P0) lethality of *Scrib Δ/Δ* mice (Pearson et al., 2015), we analyzed fetal livers at day 13.5 after conception. In these specimens, deletion of *Scrib* was associated with significantly reduced liver cellularity (Fig. 3 E). Colony-forming assays revealed the frequency of nonerythroid progenitors to be unaffected by *Scrib* status (Fig. 3 F). In contrast, the frequency of Epo-dependent BFU-E colonies was markedly diminished in *Scrib*-null samples (Fig. 3 G).

The capacity of iron-deprived erythroid progenitors to maintain survival (Bullock et al., 2010; Nai et al., 2015; Zhao et al., 2016) despite EpoR down-regulation suggested enhancement in Akt signaling, a pathway previously implicated in Epo-mediated survival (Ghaffari et al., 2006). To examine this possibility, primary erythroblasts cultured overnight in iron-replete or iron-free medium underwent cytokine starvation followed by Epo stimulation. As previously observed (Fig. 1 B), iron deprivation compromised Epo induction of STAT5 phosphorylation (Fig. 3 H). In contrast, Epo induction of Akt phosphorylation was unimpaired in iron-deprived cells (Fig. 3 H). Similar studies in HUDEP-2 erythroblasts showed that iron deprivation actually enhanced the Epo induction of Akt phosphorylation while blunting the induction of STAT5 phosphorylation (Fig. 3 I). Prior studies have shown that Scribble, through recruitment of the phosphatases PHLPP1 and PTEN, acts as an inhibitor of Akt signaling (Li et al., 2011; Feigin et al., 2014; Chen et al., 2016). Consistent with this role, Scribble knockdown in erythroid progenitors induced Akt hyperphosphorylation, despite the concurrent down-regulation of EpoR levels (Fig. 3 J). Thus, for Akt signaling, Scribble down-regulation has both negative (decreased surface EpoR) and positive (decreased phosphatase recruitment) consequences that offset one another.

Scribble and TfR2 are regulated by a shared pathway in erythroid iron deprivation

The cathepsin-dependent down-regulation of Scribble in response to iron deprivation (Fig. 2 E and Fig. S2 E) suggested involvement of lysosomal catabolism. A prior study of TfR2 in hepatoma cells has shown that its destabilization in response to holotransferrin withdrawal occurs as a result of enhanced lysosomal trafficking (Johnson and Enns, 2004). Our analysis of protein decay rates in cycloheximide-treated erythroblasts confirmed the destabilization of TfR2, but not TfR1, by iron deprivation (Fig. 4 A). Notably, isocitrate treatment completely abrogated the destabilization caused by iron deprivation (Fig. 4, A and B). As expected for a factor regulated by lysosomal catabolism, treatment of cells with the cathepsin inhibitor CA074me robustly increased TfR2 levels under both iron-replete and iron-deficient conditions (Fig. 4 C), a finding replicated in three independent experiments (Fig. S4 A). This treatment also reversed the block in GPA up-regulation associated with iron deficiency, implicating lysosomal catabolism as an integral component of the erythroid iron deprivation response (Fig. 4 D).

The parallel regulation of TfR2 and Scribble by iron, isocitrate, and cathepsin (Fig. S2 E and Fig. S4 A) raised the possibility of their participation in a protein complex. Supporting this notion, immunoprecipitation (IP) of endogenous TfR2 from K562 erythroleukemic cells efficiently coprecipitated Scribble, whereas IP of TfR1 did not (Fig. 4 E). This interaction was retained in the presence of iron chelation or aconitase inhibition and was also readily detectable in nontransformed HUDEP-2 erythroblasts (Fig. 4 F, lanes 4 and 5). Prior findings of TfR2 interacting with EpoR (Forejtnikovà et al., 2010) also raised the possibility of a Scribble–EpoR interaction. Such an interaction was confirmed by Scribble coprecipitation with endogenous EpoR in HUDEP-2 erythroblast cells (Fig. 4 F). This Scribble–EpoR interaction showed a minor but reproducible decrease associated with iron deprivation. Immunofluorescence experiments on primary erythroblasts provided evidence of EpoR colocalization with Scribble both at the plasma membrane and in cytoplasmic clusters that likely represent Golgi (Fig. S4 B). These studies further showed loss of membrane localization for both factors occurring with iron deprivation. Because of a lack of antibodies suitable for endogenous Scribble IP, additional experiments were conducted with epitope-tagged factors expressed in HEK293 transfectants. These experiments

Figure 2. **Scribble is regulated by the erythroid iron deprivation response and controls surface EpoR display. (A)** Heat map of *SCRIB* expression levels in hematopoietic hierarchy from BloodSpot server using normal human hematopoietic DMAP dataset. **(B)** Immunoblot of cytosolic (Cy), membranous (Me), and residual insoluble (In) fractions from progenitors cultured in erythroid medium at indicated TSATs ± isocitrate and densitometry from multiple experiments for relative, normalized levels of membranous and cytosolic Scribble ($n = 3$ for each, one-way ANOVA). **(C)** Immunofluorescence localization of Scribble in progenitors cultured in erythroid medium with the indicated TSATs ± isocitrate (confocal microscopy). Representative results from three independent experiments. Bar, 15 µm. **(D)** Quantitative RT-PCR measurements of relative, normalized *SCRIB* transcripts in human progenitors cultured in erythroid medium with indicated TSATs ± isocitrate ($n = 3$). IC, isocitrate. **(E)** Immunoblots of cytosolic and membrane fractions from progenitors cultured in erythroid medium with the indicated TSATs ± cathepsin inhibitor (CA074me). Representative results from three independent experiments (Fig. S2 E). **(F)** Immunoblot of surface-biotinylated proteins (streptavidin pull-down) and of input lysates (Input) from primary progenitors transduced with lentiviral shRNA control or Scribble-targeting constructs and densitometry from multiple experiments for relative levels of total EpoR, expressed as fold change associated with Scribble knockdown, with normalization to tubulin ($n = 3$, Student's *t* test). **(G)** Immunoblot of surface-biotinylated proteins (streptavidin pull-down), input lysates (Input) from HUDEP-2 erythroblasts transduced with lentiviral shRNA control and Scribble-targeting constructs, and densitometry from multiple experiments as in left panel for fold change in surface EpoR associated with Scribble knockdown normalized to total surface-biotinylated proteins ($n = 3$, Student's *t* test). EV, empty vector, lentiviral shRNA control; PD, pull-down; shScrib, Scribble-targeting lentiviral shRNA constructs. Graphs depict mean ± SEM from the indicated number of independent experiments. *, $P < 0.05$; ***, $P < 0.001$.

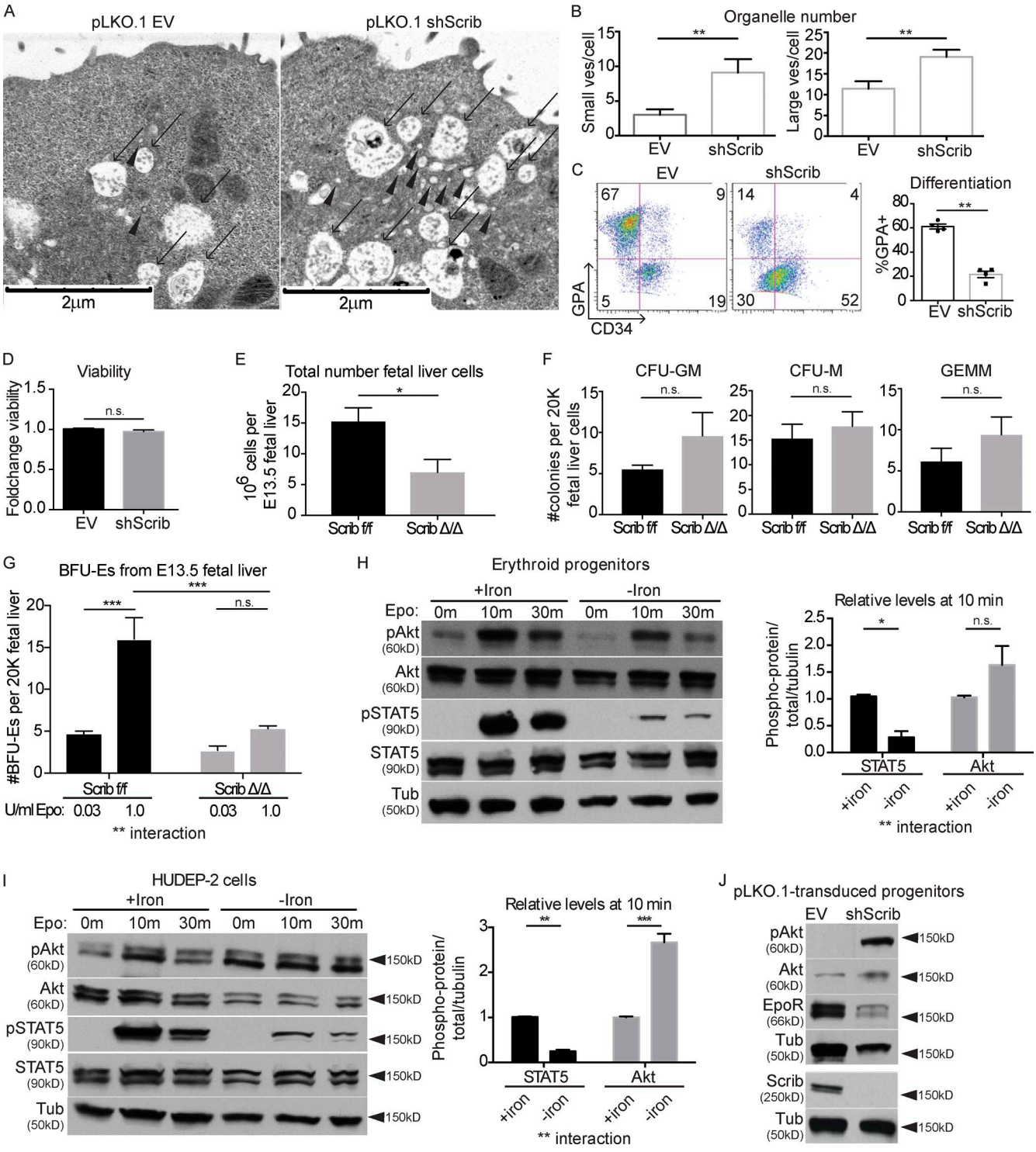

Figure 3. **Scribble regulates erythropoiesis, and its deficiency phenocopies characteristics of the erythroid iron deprivation response. (A)** EM of progenitors transduced with control or Scribble-targeting lentiviral shRNA constructs. Arrows denote large vesicles containing intraluminal vesicles. Arrowheads denote small peripheral vesicles. **(B)** Quantitation of small and large vesicles from electron micrographs of transduced progenitors as in A, representing number of vesicles per cell section (number of cells counted per group = 11, Student's *t* test). **(C)** Flow cytometry of progenitors transduced as in A and cultured 4 d in erythroid medium and summary of multiple independent flow cytometry studies of transduced progenitors ($n = 4$, Student's *t* test). **(D)** Summary of flow cytometry studies of transduced progenitors as in C, depicting fold change in viability associated with Scribble knockdown ($n = 3$, Student's *t* test). **(E)** Number of viable cells per liver from E13.5 mouse embryo littermates of indicated genotype ($n = 3$ f/f and 5 Δ/Δ, Student's *t* test). **(F)** Number of CFU-granulocyte/macrophage (GM), CFU-macrophage (M), and CFU-granulocyte/erythrocyte/monocyte/megakaryocyte (GEMM) per 20,000

used bidirectional IPs to confirm the interaction of Scribble with TfR2 but not with TfR1 (Fig. S4 C). These studies also showed that the interaction of TfR2 with Scribble was enhanced by coexpression of EpoR and JAK2, raising the possibility of a multicomponent complex (Fig. S4 D); however, overexpression of these components in a nonerythroid milieu may not recapitulate their endogenous configuration.

TfR2 regulates Scribble in the erythroid iron deprivation pathway

To dissect its role in regulation of the erythroid iron deprivation response, TfR2 underwent lentiviral shRNA–mediated knockdown in primary human progenitors. In iron-replete erythroid cultures, its knockdown induced a major (3.4-fold) increase in total cellular Scribble levels (Fig. 5, A and B). Because membrane-localized Scribble represents the active form (Feigin et al., 2014; Chen et al., 2016), we next focused on the contribution of TfR2 to modulation of membrane Scribble in the erythroid iron deprivation response. Results shown in Fig. 2 demonstrate that membrane Scribble undergoes down-modulation during erythroid iron deprivation but can be rescued by treatment of cells with isocitrate or cathepsin inhibitor. We therefore subjected control and TfR2 knockdown progenitors to iron deprivation alone or with these rescue treatments. In these experiments, TfR2 deficiency completely abrogated Scribble modulation by iron restriction and by cathepsin inhibitor or isocitrate (Fig. 5, C–F). To determine the phenotypic consequences of these alterations, transduced progenitors were analyzed by flow cytometry, and TfR2 knockdown was found to eliminate GPA modulation by iron restriction and isocitrate (Fig. 5, G and H). Therefore, TfR2 plays an essential role in the modulation of Scribble and in the phenotypic changes associated with the erythroid iron deprivation response.

Blockade of isocitrate production impairs TfR2 surface delivery

To further explore the mechanism by which isocitrate affects TfR2 catabolism (Fig. 4, A and B), erythroid progenitors underwent overnight aconitase inhibition followed by analysis of TfR2 trafficking. Initial experiments examined surface TfR2 turnover rates using pulse-chase analysis of surface-biotinylated proteins. This approach revealed, unexpectedly, no effect of aconitase inhibition on degradation of surface TfR2 (Fig. 6, A and B). An alternative mechanism for enhanced catabolism could occur through lysosomal shunting of TfR2 export vesicles. To address this possibility, erythroid progenitors underwent a stripping of surface TfR2 by transient, light trypsinization followed by incubation under erythroid culture conditions. At various intervals, recovering surface TfR2 levels were assessed by surface biotinylation followed by streptavidin pull-down and immunoblot as in Fig. 1 A. This approach revealed that the restoration of surface TfR2 was significantly impaired by aconitase inhibition, with inhibitor-treated cells failing to recover normal surface levels even after long-term cultures (Fig. 6, C–E). These findings, coupled with the results in Fig. 4 (A and B), suggest an influence of isocitrate on trafficking patterns of TfR2, with blocked production potentially rerouting export vesicles from a cell surface destination to lysosomes.

DISCUSSION

A model for erythroid coupling of iron availability with Epo responsiveness is shown in Fig. 7. The top two panels highlight an iron/isocitrate-regulated vesicle transport pathway in which TfR2 trafficking patterns influence Scribble levels and Scribble levels in turn regulate EpoR surface delivery. This pathway is supported by several key findings: (a) TfR2 undergoes enhanced lysosomal catabolism with iron deprivation, and isocitrate blocks this effect (Fig. 4); (b) TfR2 surface trafficking relies on the activity of iron-dependent aconitase enzymes (Fig. 6); (c) TfR2 binds Scribble and mediates its lysosomal catabolism in the iron deprivation response (Fig. 4 and Fig. 5); (d) Scribble interacts with EpoR and promotes its surface delivery (Fig. 2 and Fig. 4); (e) Scribble down-regulation decreases surface EpoR display, as is seen in erythroid iron deprivation (Fig. 1 and Fig. 2). Therefore, TfR2 is proposed to function in this pathway as an upstream sensor, whereas Scribble serves as an intermediary transducing element, and EpoR consists of the effector target. It is possible that Scribble down-regulation may affect delivery of other receptors to the cell surface. However, the levels of most of the surface-biotinylated proteins did not decline with erythroid iron deprivation (Fig. 1 and Fig. S1 A). Although these panels depict separate TfR2–Scribble and Scribble–EpoR complexes, it is possible that complexes may contain all three factors.

The bottom two panels in Fig. 7 depict the signaling consequences of Scribble down-regulation in the context of iron deprivation. Increased circulating levels of Epo are

fetal liver cells cultured in methylcellulose colony formation medium (n = 3 f/f and 5 Δ/Δ, Student's t test). **(G)** Number of BFU-E per 20,000 fetal liver cells cultured in methylcellulose colony formation medium with 0.03 or 1.0 U/ml Epo (n = 3 f/f and 5 Δ/Δ, two-way ANOVA). **(H)** Immunoblot analysis of primary erythroid progenitors subjected to iron deprivation and Epo stimulation and densitometry from multiple experiments for normalized differences in protein phosphorylation caused by iron deprivation in cells treated with Epo for 10 min (n = 3, two-way ANOVA). **(I)** Immunoblot analysis of HUDEP-2 erythroblasts subjected to iron deprivation and Epo stimulation and densitometry from multiple experiments for normalized differences in protein phosphorylation caused by iron deprivation in cells treated with Epo for 10 min (n = 3, two-way ANOVA). **(J)** Immunoblot of whole cell lysates from progenitors transduced with control or Scribble-targeting lentiviral shRNA constructs and cultured in iron-replete erythroid medium. Graphs depict mean ± SEM from the indicated number of independent experiments. *, P < 0.05; **, P < 0.01; ***, P < 0.001. n.s., not significant. EV, lentiviral shRNA control; shScrib, Scribble-targeting lentiviral shRNA construct.

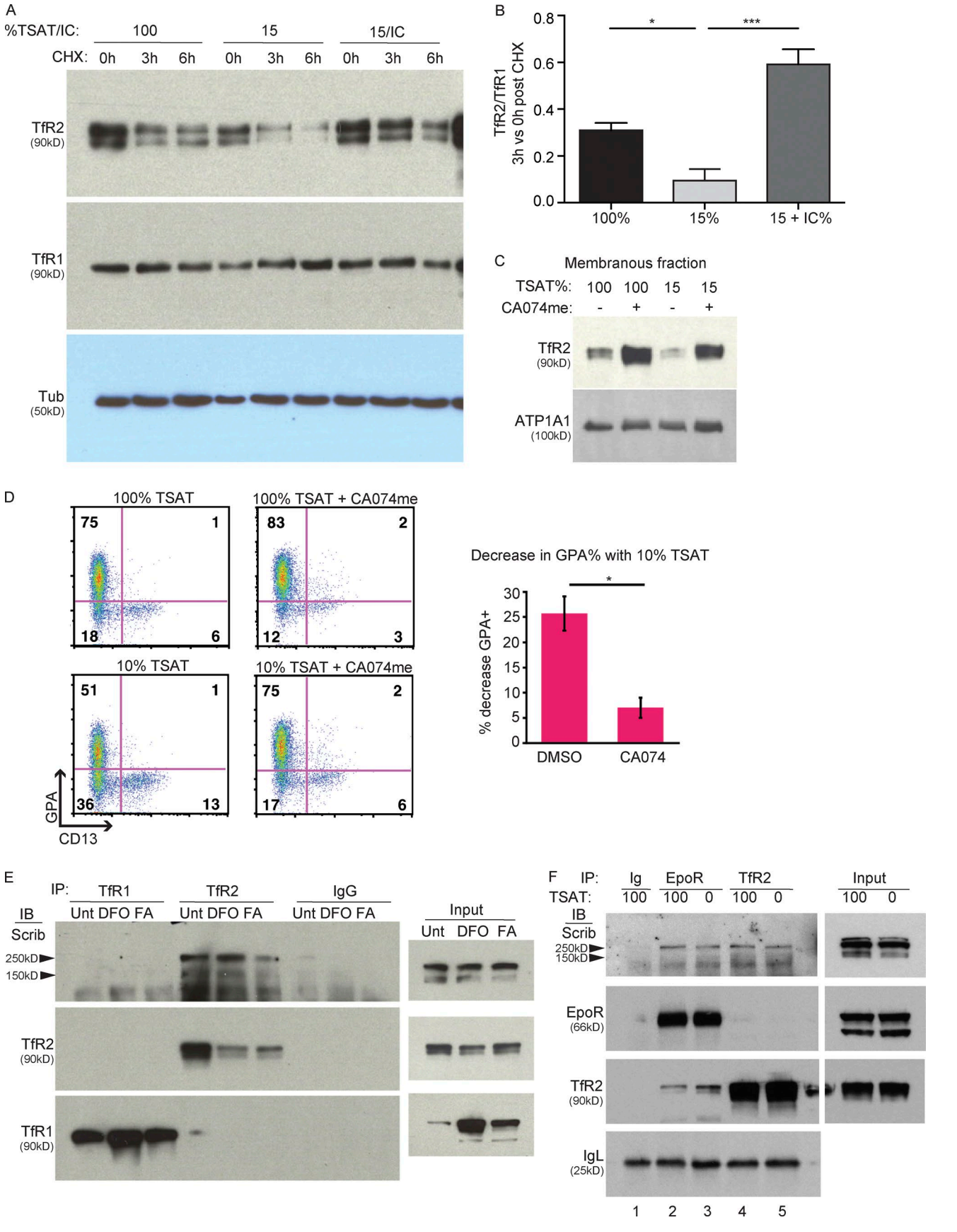

depicted because of its known up-regulation with IDA. The decrease in erythroid surface EpoR associated with iron deficiency is expected to diminish signaling via downstream pathways including JAK2–STAT5 and Akt. However, Scribble also functions as an inhibitor of Akt signaling. Therefore, iron deprivation–mediated Scribble down-regulation is expected to have both positive and negative consequences for Akt, but only negative consequences for JAK2–STAT5. This notion is supported by our finding that iron deprivation impairs Epo activation of JAK2–STAT5 but preserves or enhances Epo activation of Akt (Fig. 3).

The iron-sensing pathway depicted in Fig. 7 is proposed to act in conjunction with several previously characterized iron regulatory mechanisms. These mechanisms include the classical binding of iron response proteins to cis-acting iron response elements in transcripts relevant to iron metabolism, such as *FTH*, *FPN*, *TFRC*, and *EPAS1* (Muckenthaler et al., 2017). In addition, erythroid sensing of heme iron by several factors including the transcriptional repressor BACH1, the heme-regulated eIF2-α kinase (HRI), and the erythroid transcription factor GATA1 insures that heme and globin production maintain their balance, loss of which impairs differentiation (Chen, 2014; Tanimura et al., 2016; Yang et al., 2016). The modulation of Scribble by iron availability adds a new layer of regulation at the level of cytokine receptor transport.

Morphological studies of human clinical samples have suggested an association of IDA with abnormal vesicular trafficking in erythroid cells. Notably, EM on marrow erythroblasts from subjects with or without IDA identified markedly increased void ropheocytotic–like cytoplasmic vesicles as the principal ultrastructural abnormality associated with IDA (Rozman et al., 1992). In peripheral blood smears, abnormal erythrocytes with submembranous vacuoles, called prekeratocytes, represented the most reliable light microscopic feature for distinguishing IDA from other microcytic anemias (Harrington et al., 2008). Interestingly, Scribble deficiency in *Drosophila* imaginal disks strongly increased the numbers of Rab5-positive early endosomes (Igaki et al., 2009). As the hub in a regulatory network controlling endosomal trafficking and sorting (Sun et al., 2009; Lohia et al., 2012), Scribble thus offers a plausible molecular target in the erythroid vesicular pathology of IDA. Importantly, direct Scribble knockdown in human erythroid progenitors sufficed to recapitulate the ultrastructural abnormalities of IDA (Fig. 3, A and B).

With regard to EpoR expression on the cell surface, prior studies have shown that ∼95% of the receptor molecules in a given cell reside in intracellular pools that fail to undergo constitutive export, a property distinct from other cytokine receptors (Hilton et al., 1995; Becker et al., 2010). The manner in which EpoR surface density is regulated has remained obscure, with proposed contributions coming from ligand-dependent and -independent mechanisms (Becker et al., 2010; Singh et al., 2012). Our results reveal iron availability to be a critical influence on EpoR surface density and show that Scribble levels function as a molecular determinant of this parameter. Previous studies have shown TfR2 to bind EpoR and promote its surface export (Forejtnikovà et al., 2010). Our results suggest that this function could be exerted through the recruitment of Scribble. However, our knockdown studies in human progenitors suggest a more stringent requirement for Scribble than for TfR2 in erythropoiesis. Furthermore, mouse studies on TfR2 loss of function have provided conflicting results, one suggesting increased and another supporting decreased erythroid Epo sensitivity (Forejtnikovà et al., 2010; Nai et al., 2015). An important feature distinguishing mouse from human erythropoiesis consists of a mouse-specific Epo signaling axis that suppresses lysosomal function through up-regulation of the antiprotease Spi2A (Dev et al., 2013). Thus, the complex interplay between iron regulation of TfR2 lysosomal trafficking and Epo regulation of lysosomal function could contribute to disparate functional results based on subtle differences in model systems. Our findings ultimately support the model of Nai et al. (2015) that TfR2 in erythroid cells mediates the Epo resistance associated with iron deficiency. We further propose that Scribble, in its regulation of EpoR, represents a key downstream target in this pathway. However, TfR2 may also directly regulate EpoR, promoting surface delivery in the presence of iron and degradation in its absence.

Epo is the principal cytokine driving erythropoiesis, and one of its primary actions is to promote effective erythropoiesis by preventing apoptosis (Koury and Bondurant, 1990). A clinical hallmark of iron-restricted anemias (IDA and anemia of chronic disease and inflammation) consists of resistance to endogenous and exogenous Epo (Drüeke, 2001; Elliott et al., 2009). However, despite their Epo insensitivity, iron-deprived

Figure 4. **TfR2 stability is regulated by iron, isocitrate, and cathepsin activity. (A)** Immunoblot of whole cell lysates from human progenitors cultured in iron-replete (100% TSAT) or -deficient (15% TSAT) erythroid medium ± isocitrate and treated with cycloheximide (CHX). **(B)** Densitometry for fraction of residual TfR2 at 3 versus 0 h of cycloheximide, with normalization to TfR1 ($n = 3$, one-way ANOVA). IC, isocitrate. **(C)** Immunoblot of membrane fractions from progenitors cultured in erythroid medium with indicated TSATs ± the cathepsin inhibitor CA074me. Representative results from three independent experiments (Fig. S4 A). **(D)** Plots from flow cytometry of progenitors cultured in erythroid medium with indicated TSATs ± cathepsin inhibitor. Graph depicts percent decrease in GPA expression associated with iron deprivation ± cathepsin inhibition ($n = 3$, Student's t test). **(E)** IP of endogenous TfR1 and TfR2 using extracts from K562 cells untreated (Unt) or cultured with DFO or with FA followed by immunoblot detection. Right, input immunoblot. Representative results from three independent experiments. **(F)** IP of endogenous EpoR and TfR2 from extracts of HUDEP-2 cells cultured ± overnight iron withdrawal followed by immunoblot detection. Right, input immunoblot. Representative results from two independent experiments. IB, immunoblot. Graphs depict mean ± SEM from the indicated number of independent experiments. *, $P < 0.05$; ***, $P < 0.001$.

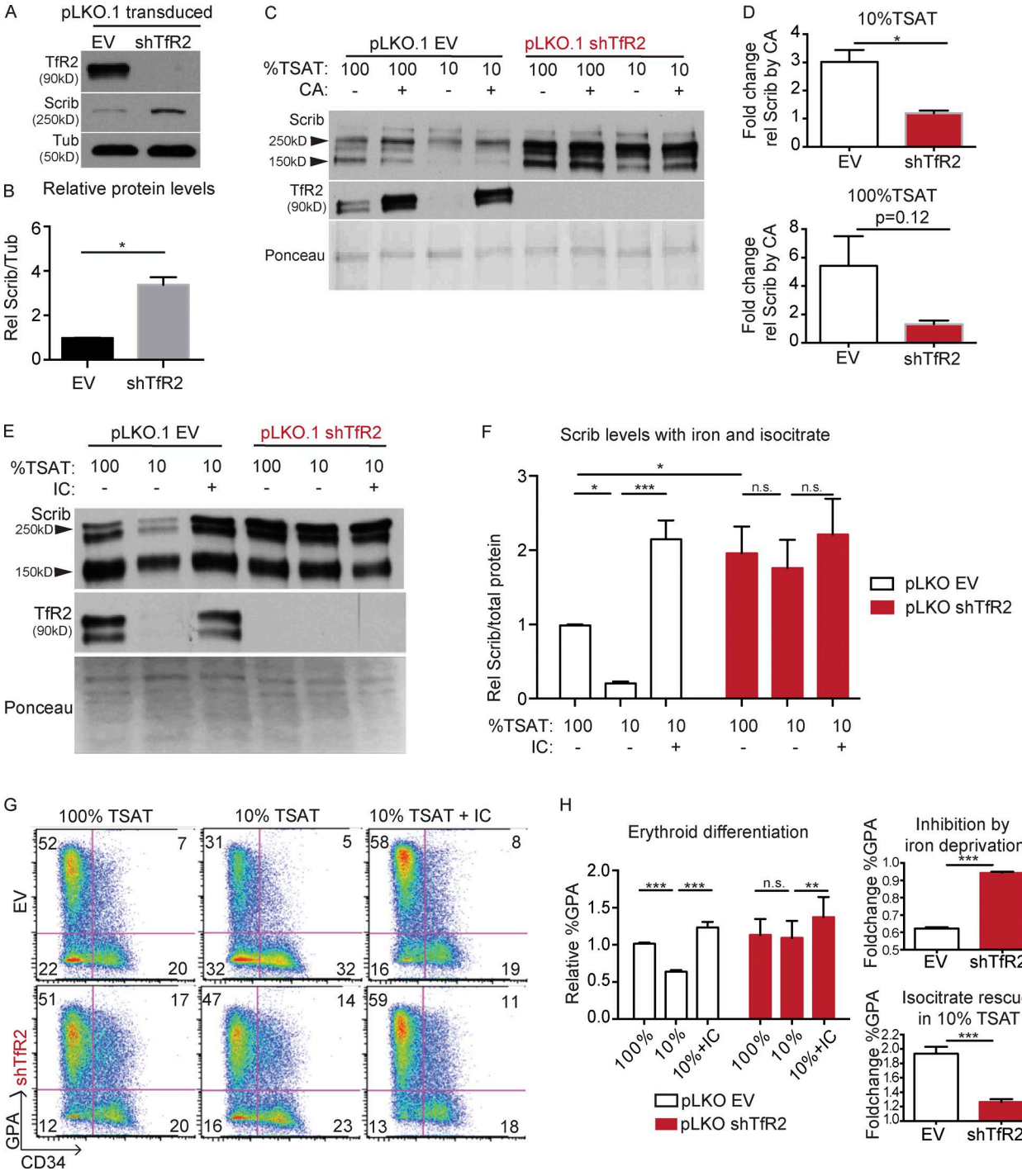

Figure 5. **TfR2 regulates Scribble and the iron deprivation response. (A)** Immunoblot of whole cell lysates from progenitors transduced with control or TfR2-targeting lentiviral constructs and cultured in iron-replete erythroid medium. **(B)** Graph of densitometry from multiple experiments as in A, reflecting 3.4-fold increase in levels of Scribble associated with TfR2 knockdown, with normalization to tubulin (Tub; $n = 3$, one-way ANOVA). **(C)** Immunoblot of membrane fractions from progenitors transduced with control or TfR2-targeting lentiviral shRNA constructs and cultured in erythroid medium with indicated TSATs ± cathepsin inhibitor. **(D)** Graphs of densitometry from multiple experiments as in C, comparing the impact of cathepsin inhibition on Scribble levels in progenitors ± TfR2 knockdown and iron deprivation as indicated, with normalization to total Ponceau signal ($n = 3$, Student's t test). CA, cathepsin. **(E)** Immunoblot of membrane fractions from progenitors transduced with control or TfR2-targeting lentiviral shRNA constructs and cultured in erythroid medium with indicated TSATs ± isocitrate. **(F)** Graph of densitometry from multiple experiments as in E for relative Scribble levels, with normalization to total Ponceau signal ($n = 3$, two-way ANOVA). **(G)** Flow cytometry of progenitors transduced with control or TfR2-targeting lentiviral shRNA constructs and cultured in erythroid medium with indicated TSATs ± isocitrate. **(H)** Graphic summary of multiple flow cytometry studies as in G, showing fold change in the

erythroid progenitors do not manifest ineffective erythropoiesis and show no increase in apoptosis (Dörmer and Lau, 1978; Rozman et al., 1992; Tanno et al., 2008; Bullock et al., 2010; Nai et al., 2015). Our work reconciles this paradox by demonstrating a reconfiguration of EpoR signaling associated with iron deprivation: decreases in surface receptor expression causing diminished STAT5 phosphorylation but unchanged or enhanced Akt phosphorylation. This reconfiguration reflects Scribble's opposing roles in positively regulating cell surface transport of receptors (Lahuna et al., 2005; Michaelis et al., 2013; Piguel et al., 2014) while negatively affecting downstream survival signaling (Nagasaka et al., 2010, 2013; Li et al., 2011). Thus, the down-regulation of Scribble associated with iron deprivation represents a novel nutrient/metabolic response that concurrently desensitizes growth signaling and sensitizes survival signaling via a common cytokine receptor. Such a response offers an adaptive advantage by maintaining a viable pool of erythroid progenitors poised to reconstitute erythropoiesis upon iron repletion.

MATERIALS AND METHODS

Cell culture

Purified normal human donor $CD34^+$ progenitors derived from G-CSF–mobilized peripheral blood mononuclear cells were purchased from Fred Hutchinson Cancer Research Center (FHCRC). These cells were obtained through a National Heart, Lung, and Blood Institute–funded core facility (HL66947) that has received approval from the FHCRC Institutional Review Board. After thawing, these cells were cultured for 72 h in prestimulation medium consisting of IMDM (GIBCO BRL) with BIT 9500 supplement (BITS; Stem Cell Technologies) and a cytokine mix comprising 100 ng/ml human stem cell factor (SCF; PeproTech), 100 ng/ml human *FMS*-like tyrosine kinase 3 ligand (PeproTech), 100 ng/ml human thrombopoietin (PeproTech), and 20 ng/ml human IL-3 (PeproTech). After prestimulation, the cells were moved to erythroid medium consisting of IMDM with 2 mM L-glutamine (Thermo Fisher Scientific), Chelex-100–stripped 0.05% BSA (Sigma-Aldrich), insulin-transferrin-selenium (ITS) supplement (Stem Cell Technologies), 0.0012% 1-thioglycerol (Sigma-Aldrich) recombinant human Epo at 4.5 U/ml (Procrit), and 25 ng/ml human SCF. Where indicated, isocitrate (DL-trisodium salt isocitric acid; Sigma-Aldrich) was included at a concentration of 20 mM. Modulation of TSAT was performed by combining holotransferrin ITS-A (Stem Cell Technologies) and apo-transferrin ITS-B (Stem Cell Technologies) at the appropriate ratios. For most experiments, cells underwent analysis after 3–5 d of erythroid culture.

For analysis of TfR2 turnover rates, primary human $CD34^+$ progenitors previously cultured for 3 d in erythroid medium were treated with cycloheximide (Cell Signaling Technology) at 75 µg/ml for the indicated durations followed by immunoblot analysis. For treatment with cathepsin inhibitor, primary human progenitors underwent culture for the indicated durations in erythroid medium supplemented with 5 µM CA074me (PI-126; Enzo Life Sciences) or DMSO only as solvent control. For endogenous IP experiments, K562 cells were treated for 16 h with 50 µM FA (Sigma-Aldrich) or 50 µM desferrioxamine (DFO; Sigma-Aldrich). For analysis of the effects of iron deprivation on Epo signaling, primary human progenitors cultured for 3 d in standard erythroid medium were moved into iron-replete versus iron-deficient (100% vs. 0% TSAT) erythroid medium for 16 h. HUDEP-2 cells were cultured in HUDEP-2 medium (described below) with doxycycline withdrawal for the last 24 h of culture, ± iron deprivation for 16 h. For Epo stimulation, both primary and HUDEP-2 cells underwent 3 h of cytokine deprivation followed by Epo treatment at 4.5 U/ml for the indicated durations and then immunoblot analysis of whole cell lysates.

K562 cells (ATCC) were grown in RPMI medium (Thermo Fisher Scientific) with 10% FBS (Thermo Fisher Scientific), 2 mM L-glutamine, and antibiotic supplement (Anti-Anti; Thermo Fisher Scientific). HEK293T cells (ATCC) were grown in DMEM with 10% FBS, 2 mM L-glutamine, and antibiotic supplement. HUDEP-2, a non-transformed, immortalized human umbilical cord blood erythroid progenitor cell line, was derived as described previously (Kurita et al., 2013). HUDEP-2 cells were cultured in serum-free expansion medium (StemSpan; Stem Cell Technologies) with 50 ng/ml human SCF, 3 U/ml Epo (Procrit), 1 µM dexamethasone (Sigma-Aldrich), and 1 µg/ml doxycycline (Sigma-Aldrich).

Flow cytometry

For flow cytometry, cells were centrifuged, washed, and resuspended in PBS with 1% FBS and conjugated antibody cocktail mix. Antibodies were added at 2 µl per 100 µl of sample, which also contained a 1:100 dilution of violet dye (Zombie; BioLegend). After 30 min of staining on ice, the samples were washed with PBS with 1% FBS and run on an ADP analyzer (CyAn; Beckman Coulter) or a flow cytometer (FACSCalibur; BD). Data analysis used the FlowJo 8.8.7 software package, which was used for compensation and gating of live cells (based on FSC/SSC and Zombie exclusion). Fluorochrome-conjugated monoclonal antibodies to human markers (CD235a, CD36, CD13, and CD34) and mouse markers (Ter119 and CD71) were purchased from BD PharMingen.

percentage of GPA+ cells normalized to empty vector–transduced cells cultured in medium with 100% TSAT, fold change in the GPA percentage associated with iron deprivation, and fold increase in the GPA percentage associated with isocitrate treatment of iron-deprived cells ($n = 4$; left, two-way ANOVA; right, Student's t test). EV, control; IC, isocitrate; shTfR2, TfR2-targeting lentiviral shRNA constructs. Graphs depict mean ± SEM from the indicated number of independent experiments. *, $P < 0.05$; **, $P < 0.01$; ***, $P < 0.001$; n.s., not significant.

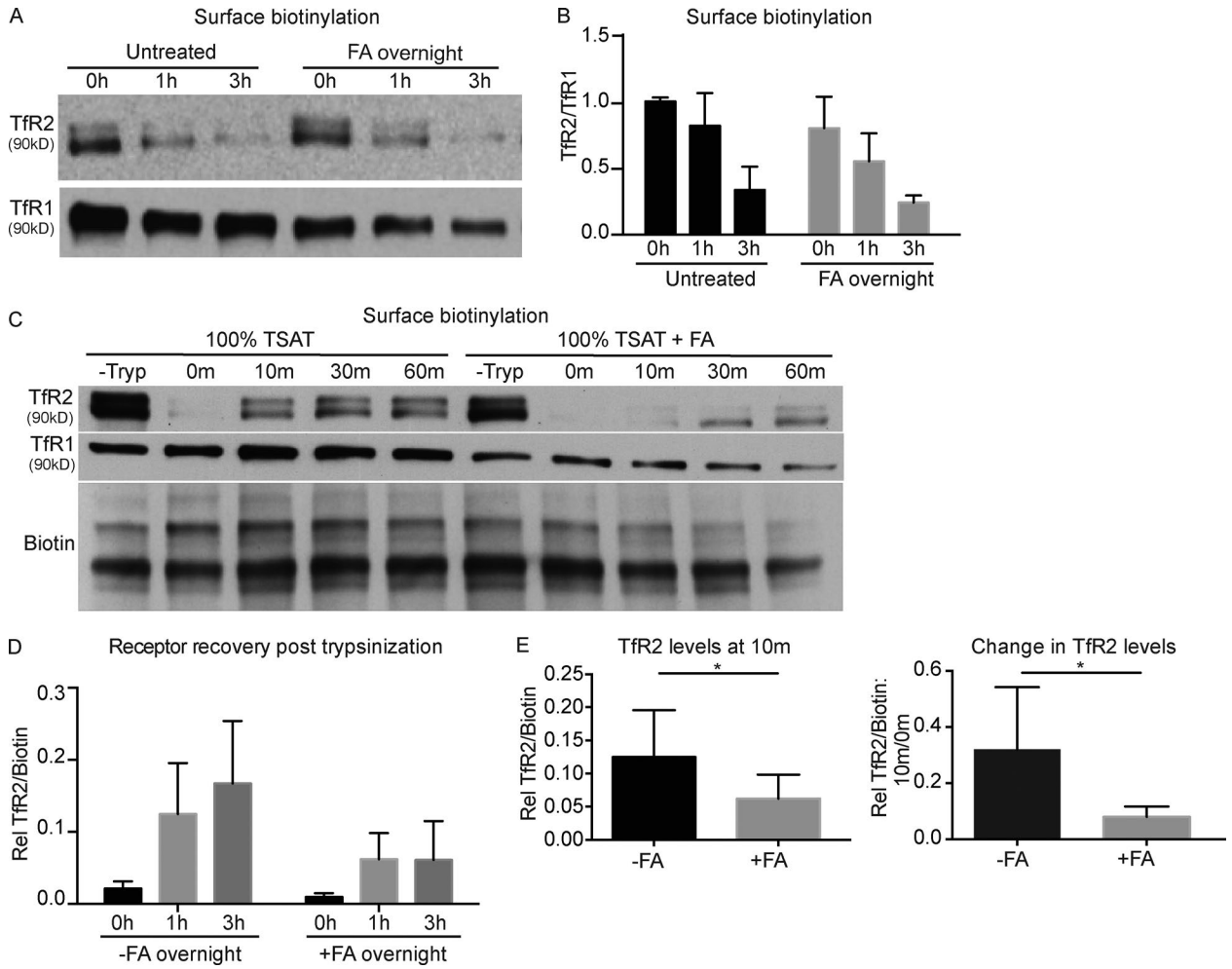

Figure 6. **Blockade of isocitrate production impairs TfR2 surface delivery. (A)** Pulse-chase analysis of surface-biotinylated TfR2 in erythroid progenitors, with assessment of the effects of aconitase inhibition. Cells cultured in erythroid medium ± 50 µM FA underwent surface biotinylation and were returned to culture for the indicated durations. The cells were then harvested for streptavidin pull-down and immunoblot. **(B)** Graph of densitometry from multiple experiments as in A for relative TfR2 levels, with normalization to TfR1 ($n = 3$, no intergroup difference by two-way ANOVA). **(C)** Analysis of the surface delivery of TfR2, with assessment of the effects of aconitase inhibition. Cells cultured in erythroid medium ± FA underwent trypsin-mediated stripping of surface TfR2 followed by recovery culture for 0–60 min. The cells were then harvested for streptavidin pull-down and immunoblot. Also shown are control cells not subjected to trypsinization (−Tryp). **(D)** Graph of densitometry from multiple experiments similar to C for surface TfR2 levels at 0–3 h after trypsinization normalized to total biotinylated protein ($n = 4$). **(E)** Quantitation from multiple experiments as in C of the effect of FA treatment on surface TfR2 recovery at 10 min after trypsinization, showing TfR2 levels normalized to total biotinylated protein and fold change in normalized TfR2 from 0 to 10 min of recovery ($n = 3$, Student's t test, *, $P < 0.05$). Graphs depict mean ± SEM from the indicated number of independent experiments.

Microscopy

For immunofluorescence, cells at a density of 10^6/ml were cytospun onto glass slides (10^5 per slide) and fixed with 4% paraformaldehyde in PBS for 15 min at room temperature. Slides were washed in PBS and then permeabilized and blocked in staining buffer (0.06% Triton X-100, 2% BSA, and 2% FBS in PBS) for 1 h at room temperature. Staining was performed using rabbit anti–human Scribble (sc-28737; Santa Cruz Biotechnology) at a dilution of 1:100 in staining buffer overnight in a hybridization chamber at 4°C. Slides were washed three times with staining buffer, and Alexa Fluor 488–conjugated secondary antibody (Thermo Fisher Scientific) was applied at a dilution of 1:500 in staining buffer for 1 h at room temperature. Slides were washed three times in staining buffer and once in PBS, mounted with coverslip and medium (H-1000; Vectashield), and imaged on a confocal microscope (LSM-700; Zeiss) with a 40× oil objective. Images were analyzed by Fiji ImageJ version 2.0.0 (National Institutes of Health). For transmission EM on primary erythroid progenitors ± knockdown of Scribble, cells were washed in PBS and fixed in PBS with 2% paraformaldehyde and 2% glutaraldehyde for 20 min at room temperature. Samples were postfixed in 1% osmium tetroxide for 1 h at room temperature and then embedded and polymerized at 65°C for 24 h. 70-nm sections

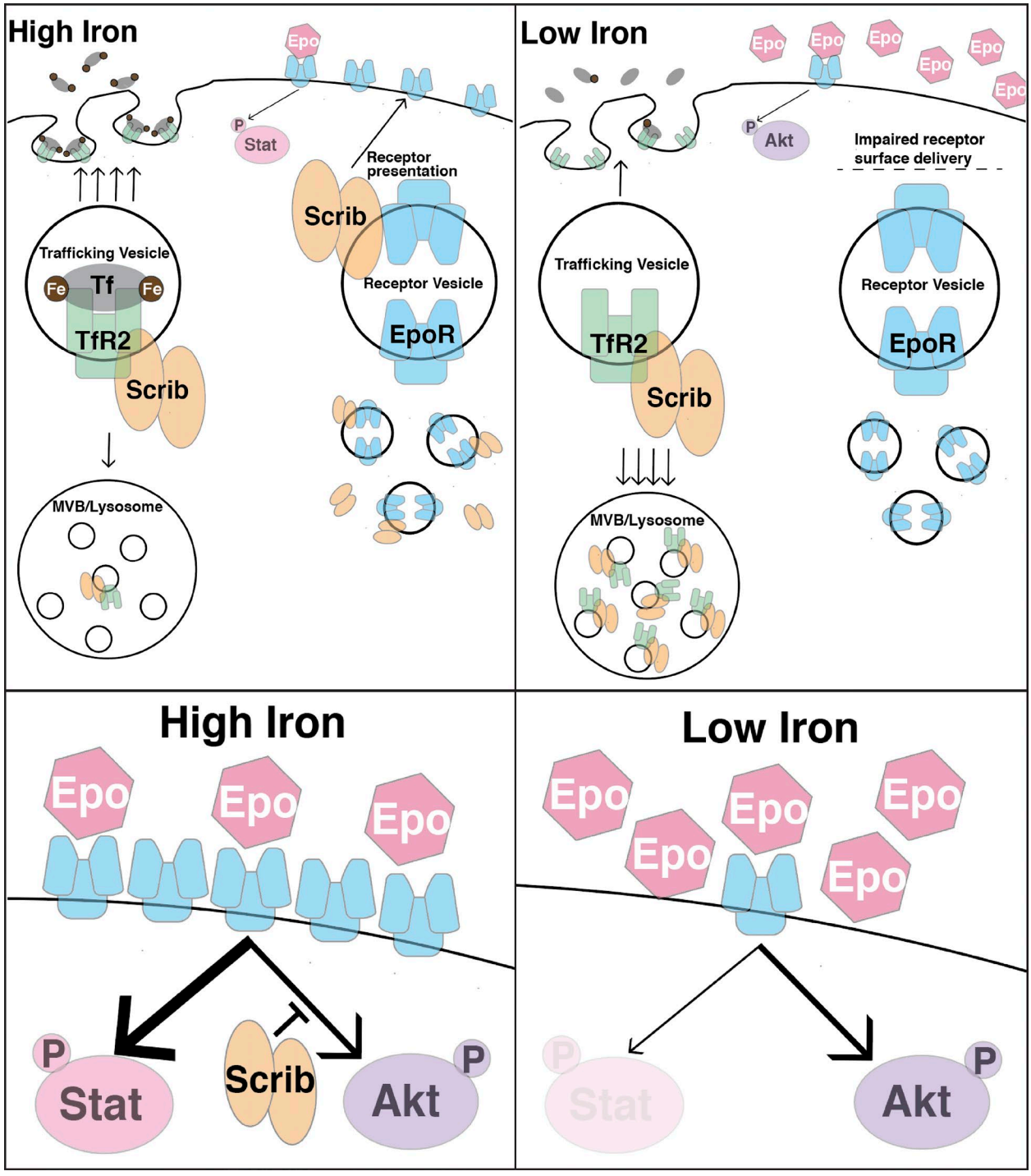

Figure 7. **A schematic model for erythroid coupling of iron availability and Epo responsiveness.** Under conditions of high iron (top left), TfR2-associated vesicles traffic predominantly to the cell surface and minimally to lysosomes. Lysosomal catabolism of TfR2–Scribble complexes occurs at a low, basal rate, permitting maintenance of critical Scribble levels. At these levels, Scribble promotes efficient EpoR surface presentation. Under conditions of low iron (top right) or aconitase inhibition, TfR2-associated vesicles traffic predominantly to lysosomes, accelerating catabolism of TfR2–Scribble complexes. As a result, Scribble levels fall below a critical threshold, impairing surface delivery of EpoR. The bottom two panels depict signaling configurations in each condition. With high iron (bottom left), high surface EpoR levels enable robust STAT5 activation, but abundant surface Scribble blunts Akt activation. With low iron (bottom right), Scribble deficiency decreases surface EpoR levels, leading to diminished STAT5 activation despite rising serum Epo levels. Akt signaling, in contrast, is preserved or even enhanced because of its liberation from Scribble inhibition. MVB, multivesicular body.

were placed on 200 mesh grids and stained with uranyl acetate and lead citrate. Grids were carbon coated to minimize conductance and imaged on an electron microscope (1230; JEOL) at 80 kV. Images were assessed in a blinded manner to quantify small circular 50–100-nm vesicles and large intraluminal vesicle-containing multivesicular bodies.

Cell extraction, fractionation, immunoblot, and IP

To produce whole cell lysates for SDS-PAGE, cell pellets were combined with equivalent volumes of 2× Laemmli sample buffer (60 mM Tris-HCl, pH 6.8, 2% SDS, 100 µM dithiothreitol, 10% glycerol, and 0.01% bromophenol blue) supplemented with protease inhibitors (cOmplete; 11836170001; Roche Diagnostics) and phosphatase inhibitors (PhosSTOP; 04906845001; Roche Diagnostics) followed by shearing of DNA and boiling for 5 min. We used a cell fractionation kit (ab109719; Abcam) for isolation of cytosolic and membrane fractions. Kit buffers and detergents were stored as frozen aliquots and supplemented with cOmplete protease inhibitors and PhosSTOP phosphatase inhibitors before cellular extraction. After electrophoresis and transfer to nitrocellulose or polyvinylidene difluoride membranes, the blots were probed overnight at 4°C or for 1 h at room temperature with primary antibodies at a 1:1,000 dilution in Tris-buffered saline with Tween 20 with 1% nonfat dried milk. HRP-conjugated secondary antibodies (Bethyl Labs) were applied for 1 h at room temperature at a 1:5,000 dilution. For global detection of biotinylated proteins, goat polyclonal antibiotin HRP conjugate (ab19221; Abcam) was used for 1 h at room temperature at a 1:5,000 dilution. HRP detection was performed using chemiluminescent SuperSignal West Pico substrate and West Femto Maximum Sensitivity substrate (both from Thermo Fisher Scientific).

Immunoblot primary antibodies consisted of the following: rabbit polyclonal anti-Scribble (4475; Cell Signaling Technology), mouse monoclonal anti–human TfR2 (sc-32271; Santa Cruz Biotechnology), rabbit polyclonal anti-EpoR (sc-695; Santa Cruz Biotechnology), rabbit polyclonal anti-TfR1 (sc-9099; Santa Cruz Biotechnology), rabbit polyclonal anti-ATP1A1 (3010; Cell Signaling Technology), rabbit polyclonal anti-STAT5 (9363S; Cell Signaling Technology), rabbit monoclonal antiphospho-STAT5 (pY694; 4322P; Cell Signaling Technology), rabbit monoclonal antiphospho-Akt (pS473; 4060S; Cell Signaling Technology), rabbit monoclonal anti-Akt (4685S; Cell Signaling Technology), mouse monoclonal antitubulin (clone DM1A; T9026; Sigma-Aldrich), and rabbit polyclonal anti-LDH (sc-33781; Santa Cruz Biotechnology). The specificity of the sc-695 anti-EpoR antibody preparation was validated by Forejtnikovà et al. (2010) and by our experiments using HEK293 transfectants (Fig. S4 D).

For IPs on K562 cells ± DFO or FA treatment, cells were washed in PBS and resuspended in IP lysis buffer (150 mM NaCl, 2 mM $MgCl_2$, 10 mM Hepes [Thermo Fisher Scientific], 0.5% NP-40, protease inhibitor, and phosphatase inhibitor) at a density of 2×10^6 cells per 100 µl. The same extraction protocol was used for IPs on HUDEP-2 cells subjected to overnight doxycycline withdrawal ± iron deprivation. For IPs on HEK293T transfectants, cells were washed and overlaid with 500 µl IP lysis buffer per semiconfluent 10-cm plate. Suspensions were incubated on ice for 15 min and centrifuged for 10 min at 15,000 rpm at 4°C. Protein content in the supernatant was quantified by bicinchoninic acid. For all IPs, 2 µg of antibody was added per milligram of protein extract in 1 ml lysis buffer followed by overnight rotation at 4°C. The following antibodies were used for IP of K562 and HUDEP-2 endogenous proteins: mouse monoclonal anti–human TfR1 (sc-32272; Santa Cruz Biotechnology), mouse monoclonal anti–human TfR2 (sc-376278; Santa Cruz Biotechnology), mouse monoclonal anti–human EpoR (38409; Thermo Fisher Scientific), and mouse IgG control (sc-2025; Santa Cruz Biotechnology). The following antibody conjugates were used for IP of epitope-tagged recombinant proteins: mouse monoclonal anti-Myc magnetic beads (5698S; Cell Signaling Technology), mouse monoclonal anti-FLAG magnetic beads (M8823; Sigma-Aldrich), and control mouse IgG magnetic beads (5873; Cell Signaling Technology). IPs with unconjugated antibodies were captured with a 1:1 mixture of magnetic beads conjugated to protein A (88846; Thermo Fisher Scientific) and to protein G (88847; Thermo Fisher Scientific), prewashed three times in lysis buffer, and added at a volume of 25 µl of packed beads per 1-ml sample. Bead suspensions were rotated for 2 h at 4°C, quickly washed twice in lysis buffer, slowly washed twice with 15 min of rotation in 4°C lysis buffer, again quickly washed twice in lysis buffer, resuspended in 50 µl Laemmli buffer, boiled, and analyzed by immunoblot as described above.

Immunoblot signals were quantified using a GS-800 calibrated densitometer (Bio-Rad). Signals were normalized using loading controls to derive relative band densities. Ponceau S–stained membranes were imaged with a membrane imager (Fluorchem HD2; Alpha Innotech), and total lane density was quantified by ImageJ. Immunoblots shown are representative of at least three independent experiments.

Cell surface biotinylation and surface TfR2 recovery after trypsinization

Cells were washed with PBS and resuspended at a density of 10^7/ml in surface-impermeable biotinylation reagent: 1 mg/ml EZ-Link Sulfo-NHS-LC-Biotin (21335; Thermo Fisher Scientific) in PBS, pH 8.0. The cell suspension was incubated on ice for 30 min and washed twice with PBS, pH 8.0, supplemented with 100 mM glycine. The cells were resuspended at a density of 10^6 cells per 150 µl in biotin lysis buffer (150 mM NaCl, 5 mM EDTA, and 10 mM Tris-HCl, pH 7.4, with 1% Triton X-100), incubated for 15 min on ice, and centrifuged at 17,000 rpm for 10 min at 4°C. A portion of supernatant was directly analyzed by immunoblot as input, and the remainder was combined with prewashed resin (NeutrAvidin; Thermo Fisher Scientific) at a ratio of 3:1 ly-

sate/bead slurry. Slurry/lysate mixtures were rotated for 1 h at 4°C, washed twice in biotin lysis buffer, and resuspended in Laemmli buffer for immunoblot analysis of eluates. For analysis of surface TfR2 recovery after trypsinization, 10^6 cells were resuspended in 100 µl of ice-cold PBS with 0.05% trypsin (Sigma-Aldrich). After incubation on ice for 20 min, the cells were washed with ice-cold IMDM and then resuspended in erythroid medium. The cells were cultured at 37°C for the indicated durations and then subjected to surface biotinylation, streptavidin pull-down, and immunoblot as described above.

Transfections and transduction

For cotransfections, HEK293T cells were grown in 10-cm plates to 60% confluency and transfected in normal culture medium with 20 µg of plasmid using a CalPhos kit (631312; Clontech). At 16 h after transfection, the medium was exchanged with fresh growth medium for protein extraction or Opti-MEM I (Thermo Fisher Scientific) for lentiviral packaging. Protein extracts for IP were obtained 40 h after initiation of transfection. For lentiviral vector packaging, supernatants were collected 40 h after initiation of transfection.

Lentiviral packaging plasmids pCMV-dR8.74 (GAG POL TAT REV) and pMD2.G (VSV-G) were cotransfected with pLKO.1 shRNA vectors via calcium phosphate precipitation into HEK293T cells as above. A mass ratio of 3:1:4 for pCMV-dR8.74/pMD2.G/pLKO.1 was used for transfection. pLKO.1 vectors expressing shRNAs active against the following human targets were purchased (GE Dharmacon): *SCRIB* (TRCN0000004457 and TRCN0000004458) and *TFR2* (TRCN0000063628 and TRCN0000063630). Viral supernatants were filtered with 0.45-µm syringe filters and stored at −80°C. K562 cells were incubated with viral supernatants for 24 h, followed by puromycin selection at 2 µg/ml in growth medium for 48 h. HUDEP-2 cells were incubated for 24 h in viral supernatants supplemented with 50 ng/ml human SCF, 3 U/ml Epo, 1 µM dexamethasone, and 1 µg/ml doxycycline, followed by puromycin selection at 2 µg/ml in HUDEP-2 media for 72 h. For human primary progenitors, cells were expanded in prestimulation medium for 48 h and transferred to retronectin-coated 12-well plates containing viral supernatants supplemented with prestimulation cytokines. After 2 h at 37°C, the plates were spun at 500 *g* for 90 min and then returned to 37°C. After overnight culture, the cells were transferred to fresh viral supernatants with prestimulation cytokines and subjected to a second round of spinoculation and overnight culture followed by selection with 2 µg/ml puromycin in prestimulation medium. After 48 h of puromycin selection, live cells were enriched by centrifugation on Ficoll-Paque PLUS medium (17-1440-02; GE Healthcare) and washed in IMDM. Viable mononuclear cells were then subjected to erythroid cultures as described above.

The following expression constructs were used for cotransfection and co-IP: pcDNA6/myc-his human and mouse TfR1 and TfR2 from P. Schmidt (Boston Children's Hospital, Boston, MA); pcDNA3-FLAG human Scribble from I. Macara (Vanderbilt University School of Medicine, Nashville, TN); and pcDNA3-Human-EpoR and human-JAK2 from F. Verdier (Institut Cochin, Université Paris Descartes, Centre National de la Recherche Scientifique, Paris, France) and O. Bernard (Université René Descartes), respectively.

Mouse models

All animal experiments were approved by the University of Virginia Institutional Animal Care and Use Committee. The *EpoR-H* mouse strain on a BALB/c background was provided by J. Ihle (St. Jude Children's Research Hospital, Memphis, TN). This strain was subsequently backcrossed onto a C57BL/6J background for 10 generations. WT controls consisted of age-, sex-, and strain-matched mice purchased from Jackson Labs. Serum EPO levels were determined with the Quantikine Mouse EPO ELISA kit (R&D Systems). For dietary induction of IDA, 3-wk-old male weanlings were placed on iron-deficient chow (TD.80396 custom diet; Envigo Teklad Diets) for the duration of the experiment. Weekly retroorbital bleeds into EDTA-coated collection tubes were analyzed for complete blood counts on a hematology system (Hemavet 950; Drew Scientific Group).

For induction of erythroid stress progenitors, mice received phenylhydrazine hydrochloride (P6926; Sigma-Aldrich) at 60 mg/kg/d for two sequential days by intraperitoneal injection. 3 d after the second injection, spleens were isolated, passed through a 70-µm filter mesh, incubated for 5 min at room temperature in ammonium chloride lysis buffer (Thermo Fisher Scientific) to remove RBCs, and washed in PBS. The cells were then incubated with a biotinylated anti-lineage cocktail (130-090-858; Miltenyi Biotec) and lineage depleted on a column (AutoMACS Pro; Miltenyi Biotec). The resulting cells were resuspended in 100 µl of sterile PBS with 1% FBS plus 2 µl APC-conjugated anti–c-Kit and 2 µl PE-conjugated anti-Ter119 (341096; 555673; BD PharMingen). After a 30-min incubation on ice, the stained cells were washed in PBS with 1% FBS, resuspended in IMDM, and subjected to sorting on a flow cytometer (FACSVantage SE TurboSort DIVA; BD) in the University of Virginia flow cytometry core facility. The isolated Lin^- Kit^+ $Ter119^-$ progenitors were directly cultured in erythroid medium as described above, except that 100 ng/ml mouse SCF (PeproTech) was substituted for human SCF. Cells were analyzed by flow cytometry after 4 d of erythroid culture under the indicated conditions.

The *Scrib*-floxed mouse strain on a 129/Sv/CB57BL/6 background was provided by A.E. Griep (University of Wisconsin-Madison, Madison, WI; Yamben et al., 2013). Germline deletions were generated by crossing with the *EIIa-Cre* strain (Jackson Labs). E13.5 embryos from Δ/f intercrosses underwent sterile dissection of fetal livers, which were converted to single-cell suspensions via 21-gauge syringe trituration in IMDM. Control f/f samples were derived from littermates of Δ/Δ fetuses. Total cells per fetal liver were

counted and resuspended in medium (MethoCult M3534; Stem Cell Technologies) at a density of 20,000 cells per well. Epo (Procrit) was supplemented to generate a final concentration of 0.03 or 1.0 U/ml. Colonies were counted on day 7 after seeding.

RNA analysis

RNA was isolated from human erythroid progenitors using the RNeasy Plus Mini kit (QIAGEN) with DNase treatment of columns before RNA elution. RNA yield and quality were determined on a spectrophotometer (Thermo NanoDrop; Thermo Fisher Scientific). Reverse transcription was performed using the High-Capacity cDNA Reverse Transcription kit (4368814; Applied Biosystems). Quantitative PCR was performed using the iQ SYBR green assay on a CFX Connect Real-Time PCR Detection System (1708880; Bio-Rad). For relative quantitation of transcript levels, we used the comparative $\Delta\Delta C_t$ formula delineated in the ABI Prism 7700 Sequence Detection System user bulletin no. 2. All samples underwent triplicate analysis with normalization performed by subtraction of the C_t value for *GAPDH*. Primers were as follows: human *GAPDH* (forward: 5′-AGCCACATCGCTCAGACA-3′; reverse: 5′-GCCCAATACGACCAAATCC-3′) and human *SCRIB* (forward: 5′-CTGACCCTCACCATCCTG-3′; reverse: 5′-CAGAGCCACACCATTCAC-3′).

Statistics

Individual results shown are representative of at least two independent experiments. Statistical analysis was performed with Prism 6 (GraphPad Software). Graphs are displayed as the mean of independent experiments ± SEM. Data were analyzed either by two-tailed Student's *t* test, one-way ANOVA, or two-way ANOVA on a minimum of three independent experiments. Post-hoc analysis of one-way ANOVA studies was performed using Dunnett's multiple comparisons test. Post-hoc analysis of two-way ANOVA studies was performed using Sidak's multiple comparisons test.

Online supplemental material

Fig. S1 shows surface TfR1 levels in erythroid progenitors ± iron withdrawal, erythroid maturation and serum Epo levels in iron-replete *EpoR-H* versus WT mice, and erythroid maturation in iron-deprived *EpoR-H* versus WT mice. Fig. S2 shows a heat map of *Scrib* expression in mouse hematopoiesis, confirmation of three distinct protein species as Scribble, and densitometry for Scribble modulation by iron deprivation and cathepsin inhibition. Fig. S3 shows phenotypic consequences of Scribble knockdown on human erythropoiesis, as assessed by flow cytometry. Fig. S4 shows densitometry for TfR2 modulation by iron deprivation and cathepsin inhibition, immunofluorescence for Scribble and EpoR in erythroid progenitors ± iron deprivation, and interactions of epitope-tagged Scribble in HEK293 transfectants.

ACKNOWLEDGMENTS

We thank Olivier Bernard, Ian Macara, Paul Schmidt, and Frédérique Verdier for providing plasmids; Jim Ihle and Anne Griep for mouse strains; Joanne Lannigan and the University of Virginia Flow Cytometry Core Facility for assistance with flow cytometry and cell sorting; Dave Kashatus and Bettina Winckler for reviewing the manuscript; and Rob Fleming for valued advice and discussions.

This work was supported by grants from the National Institutes of Health (grants R01 DK079924, R01 DK101550, and K08 HL093355), the Leukemia and Lymphoma Society (grant LLS NIA-8988-15), the Farrow Fellowship, the National Cancer Institute Cancer Center support grant P30 CA44579, and the Medical Scientist Training Program at the University of Virginia (grant 5T32GM007267-38).

The authors declare no competing financial interests.

Author contributions: S. Khalil designed and conducted experiments, interpreted data, and wrote the manuscript. L. Delehanty designed and conducted experiments, interpreted data, and edited the manuscript. S. Grado, M. Holy, Z. White III, K. Freeman, and G. Bullock conducted experiments and edited the manuscript. R. Kurita and Y. Nakamura developed the HUDEP-2 system and edited the manuscript. A. Goldarb supervised the project, designed experiments, interpreted data, and wrote the manuscript.

Submitted: 1 March 2017

Revised: 2 June 2017

Accepted: 17 November 2017

REFERENCES

Aljitawi, O.S., S. Paul, A. Ganguly, T.L. Lin, S. Ganguly, G. Vielhauer, M.L. Capitano, A. Cantilena, B. Lipe, J.D. Mahnken, et al. 2016. Erythropoietin modulation is associated with improved homing and engraftment after umbilical cord blood transplantation. *Blood*. 128:3000–3010. https://doi.org/10.1182/blood-2016-05-715292

Bagger, F.O., D. Sasivarevic, S.H. Sohi, L.G. Laursen, S. Pundhir, C.K. Sønderby, O. Winther, N. Rapin, and B.T. Porse. 2016. BloodSpot: a database of gene expression profiles and transcriptional programs for healthy and malignant haematopoiesis. *Nucleic Acids Res.* 44(D1):D917–D924. https://doi.org/10.1093/nar/gkv1101

Becker, V., M. Schilling, J. Bachmann, U. Baumann, A. Raue, T. Maiwald, J. Timmer, and U. Klingmüller. 2010. Covering a broad dynamic range: information processing at the erythropoietin receptor. *Science*. 328:1404–1408. https://doi.org/10.1126/science.1184913

Bullock, G.C., L.L. Delehanty, A.-L. Talbot, S.L. Gonias, W.-H. Tong, T.A. Rouault, B. Dewar, J.M. Macdonald, J.J. Chruma, and A.N. Goldfarb. 2010. Iron control of erythroid development by a novel aconitase-associated regulatory pathway. *Blood*. 116:97–108. https://doi.org/10.1182/blood-2009-10-251496

Camaschella, C. 2015. Iron-Deficiency Anemia. *N. Engl. J. Med.* 373:485–486.

Chen, J.-J. 2014. Translational control by heme-regulated eIF2α kinase during erythropoiesis. *Curr. Opin. Hematol.* 21:172–178. https://doi.org/10.1097/MOH.0000000000000030

Chen, B., B. Zheng, M. DeRan, G.K. Jarugumilli, J. Fu, Y.S. Brooks, and X. Wu. 2016. ZDHHC7-mediated S-palmitoylation of Scribble regulates cell polarity. *Nat. Chem. Biol.* 12:686–693. https://doi.org/10.1038/nchembio.2119

Choi, J.W. 2007. Serum transferrin receptor concentration and its ratio to bone marrow erythroblasts in iron deficiency anemia and anemia of chronic diseases. *Ann. Clin. Lab. Sci.* 37:288–290.

Dev, A., S.M. Byrne, R. Verma, P.G. Ashton-Rickardt, and D.M. Wojchowski. 2013. Erythropoietin-directed erythropoiesis depends on serpin inhibition of erythroblast lysosomal cathepsins. *J. Exp. Med.* 210:225–232. https://doi.org/10.1084/jem.20121762

Dörmer, P., and B. Lau. 1978. Kinetics of erythroblast proliferation in states of hypoferremia. *Isr. J. Med. Sci.* 14:1144–1151.

Drüeke, T. 2001. Hyporesponsiveness to recombinant human erythropoietin. *Nephrol. Dial. Transplant.* 16(Suppl 7):25–28. https://doi.org/10.1093/ndt/16.suppl_7.25

Elliott, J., D. Mishler, and R. Agarwal. 2009. Hyporesponsiveness to erythropoietin: causes and management. *Adv. Chronic Kidney Dis.* 16:94–100. https://doi.org/10.1053/j.ackd.2008.12.004

Elsum, I.A., C. Martin, and P.O. Humbert. 2013. Scribble regulates an EMT polarity pathway through modulation of MAPK-ERK signaling to mediate junction formation. *J. Cell Sci.* 126:3990–3999. https://doi.org/10.1242/jcs.129387

Feigin, M.E., S.D. Akshinthala, K. Araki, A.Z. Rosenberg, L.B. Muthuswamy, B. Martin, B.D. Lehmann, H.K. Berman, J.A. Pietenpol, R.D. Cardiff, and S.K. Muthuswamy. 2014. Mislocalization of the cell polarity protein scribble promotes mammary tumorigenesis and is associated with basal breast cancer. *Cancer Res.* 74:3180–3194. https://doi.org/10.1158/0008-5472.CAN-13-3415

Forejtnikovà, H., M. Vieillevoye, Y. Zermati, M. Lambert, R.M. Pellegrino, S. Guihard, M. Gaudry, C. Camaschella, C. Lacombe, A. Roetto, et al. 2010. Transferrin receptor 2 is a component of the erythropoietin receptor complex and is required for efficient erythropoiesis. *Blood.* 116:5357–5367. https://doi.org/10.1182/blood-2010-04-281360

Frise, M.C., H.-Y. Cheng, A.H. Nickol, M.K. Curtis, K.A. Pollard, D.J. Roberts, P.J. Ratcliffe, K.L. Dorrington, and P.A. Robbins. 2016. Clinical iron deficiency disturbs normal human responses to hypoxia. *J. Clin. Invest.* 126:2139–2150. https://doi.org/10.1172/JCI85715

Ganz, T., and E. Nemeth. 2012. Iron metabolism: interactions with normal and disordered erythropoiesis. *Cold Spring Harb. Perspect. Med.* 2:a011668. https://doi.org/10.1101/cshperspect.a011668

Ghaffari, S., C. Kitidis, W. Zhao, D. Marinkovic, M.D. Fleming, B. Luo, J. Marszalek, and H.F. Lodish. 2006. AKT induces erythroid-cell maturation of JAK2-deficient fetal liver progenitor cells and is required for Epo regulation of erythroid-cell differentiation. *Blood.* 107:1888–1891. https://doi.org/10.1182/blood-2005-06-2304

Grover, A., E. Mancini, S. Moore, A.J. Mead, D. Atkinson, K.D. Rasmussen, D. O'Carroll, S.E.W. Jacobsen, and C. Nerlov. 2014. Erythropoietin guides multipotent hematopoietic progenitor cells toward an erythroid fate. *J. Exp. Med.* 211:181–188. https://doi.org/10.1084/jem.20131189

Gunawardena, N.D., V. Schrott, C. Richardson, T.N. Cole, C.G. Corey, Y. Wang, S.S. Shiva, and G.C. Bullock. 2016. Aconitase: an iron sensing regulator of mitochondrial oxidative metabolism and erythropoiesis. *Blood.* 128:74.

Harrington, A.M., P.C. Ward, and S.H. Kroft. 2008. Iron deficiency anemia, beta-thalassemia minor, and anemia of chronic disease: a morphologic reappraisal. *Am. J. Clin. Pathol.* 129:466–471. https://doi.org/10.1309/LY7YLUPE7551JYBG

Hilton, D.J., S.S. Watowich, P.J. Murray, and H.F. Lodish. 1995. Increased cell surface expression and enhanced folding in the endoplasmic reticulum of a mutant erythropoietin receptor. *Proc. Natl. Acad. Sci. USA.* 92:190–194. https://doi.org/10.1073/pnas.92.1.190

Igaki, T., J.C. Pastor-Pareja, H. Aonuma, M. Miura, and T. Xu. 2009. Intrinsic tumor suppression and epithelial maintenance by endocytic activation of Eiger/TNF signaling in Drosophila. *Dev. Cell.* 16:458–465. https://doi.org/10.1016/j.devcel.2009.01.002

Johnson, M.B., and C.A. Enns. 2004. Diferric transferrin regulates transferrin receptor 2 protein stability. *Blood.* 104:4287–4293. https://doi.org/10.1182/blood-2004-06-2477

Johnson, M.B., J. Chen, N. Murchison, F.A. Green, and C.A. Enns. 2007. Transferrin receptor 2: evidence for ligand-induced stabilization and redirection to a recycling pathway. *Mol. Biol. Cell.* 18:743–754. https://doi.org/10.1091/mbc.E06-09-0798

Kim, A., E. Fung, S.G. Parikh, V. Gabayan, E. Nemeth, and T. Ganz. 2016. Isocitrate treatment of acute anemia of inflammation in a mouse model. *Blood Cells Mol. Dis.* 56:31–36. https://doi.org/10.1016/j.bcmd.2015.09.007

Kimura, H., C.A. Finch, and J.W. Adamson. 1986. Hematopoiesis in the rat: quantitation of hematopoietic progenitors and the response to iron deficiency anemia. *J. Cell. Physiol.* 126:298–306. https://doi.org/10.1002/jcp.1041260221

Koury, M.J., and M.C. Bondurant. 1990. Erythropoietin retards DNA breakdown and prevents programmed death in erythroid progenitor cells. *Science.* 248:378–381. https://doi.org/10.1126/science.2326648

Kurita, R., N. Suda, K. Sudo, K. Miharada, T. Hiroyama, H. Miyoshi, K. Tani, and Y. Nakamura. 2013. Establishment of immortalized human erythroid progenitor cell lines able to produce enucleated red blood cells. *PLoS One.* 8:e59890. https://doi.org/10.1371/journal.pone.0059890

Lahuna, O., M. Quellari, C. Achard, S. Nola, G. Méduri, C. Navarro, N. Vitale, J.P. Borg, and M. Misrahi. 2005. Thyrotropin receptor trafficking relies on the hScrib-betaPIX-GIT1-ARF6 pathway. *EMBO J.* 24:1364–1374. https://doi.org/10.1038/sj.emboj.7600616

Li, X., H. Yang, J. Liu, M.D. Schmidt, and T. Gao. 2011. Scribble-mediated membrane targeting of PHLPP1 is required for its negative regulation of Akt. *EMBO Rep.* 12:818–824. https://doi.org/10.1038/embor.2011.106

Lodish, H., J. Flygare, and S. Chou. 2010. From stem cell to erythroblast: regulation of red cell production at multiple levels by multiple hormones. *IUBMB Life.* 62:492–496. https://doi.org/10.1002/iub.322

Lohia, M., Y. Qin, and I.G. Macara. 2012. The Scribble polarity protein stabilizes E-cadherin/p120-catenin binding and blocks retrieval of E-cadherin to the Golgi. *PLoS One.* 7:e51130. https://doi.org/10.1371/journal.pone.0051130

Menon, M.P., J. Fang, and D.M. Wojchowski. 2006. Core erythropoietin receptor signals for late erythroblast development. *Blood.* 107:2662–2672. https://doi.org/10.1182/blood-2005-02-0684

Michaelis, U.R., E. Chavakis, C. Kruse, B. Jungblut, D. Kaluza, K. Wandzioch, Y. Manavski, H. Heide, M.J. Santoni, M. Potente, et al. 2013. The polarity protein Scrib is essential for directed endothelial cell migration. *Circ. Res.* 112:924–934. https://doi.org/10.1161/CIRCRESAHA.112.300592

Muckenthaler, M.U., S. Rivella, M.W. Hentze, and B. Galy. 2017. A red carpet for iron metabolism. *Cell.* 168:344–361. https://doi.org/10.1016/j.cell.2016.12.034

Nagasaka, K., D. Pim, P. Massimi, M. Thomas, V. Tomaić, V.K. Subbaiah, C. Kranjec, S. Nakagawa, T. Yano, Y. Taketani, et al. 2010. The cell polarity regulator hScrib controls ERK activation through a KIM site-dependent interaction. *Oncogene.* 29:5311–5321. https://doi.org/10.1038/onc.2010.265

Nagasaka, K., T. Seiki, A. Yamashita, P. Massimi, V.K. Subbaiah, M. Thomas, C. Kranjec, K. Kawana, S. Nakagawa, T. Yano, et al. 2013. A novel interaction between hScrib and PP1γ downregulates ERK signaling and suppresses oncogene-induced cell transformation. *PLoS One.* 8:e53752. https://doi.org/10.1371/journal.pone.0053752

Nai, A., M.R. Lidonnici, M. Rausa, G. Mandelli, A. Pagani, L. Silvestri, G. Ferrari, and C. Camaschella. 2015. The second transferrin receptor regulates red blood cell production in mice. *Blood.* 125:1170–1179. https://doi.org/10.1182/blood-2014-08-596254

Pearson, H.B., E. McGlinn, T.J. Phesse, H. Schlüter, A. Srikumar, N.J. Gödde, C.B. Woelwer, A. Ryan, W.A. Phillips, M. Ernst, et al. 2015. The polarity protein Scrib mediates epidermal development and exerts a tumor suppressive function during skin carcinogenesis. *Mol. Cancer.* 14:169. https://doi.org/10.1186/s12943-015-0440-z

Piguel, N.H., S. Fievre, J.M. Blanc, M. Carta, M.M. Moreau, E. Moutin, V.L. Pinheiro, C. Medina, J. Ezan, L. Lasvaux, et al. 2014. Scribble1/AP2 complex coordinates NMDA receptor endocytic recycling. *Cell Reports.* 9:712–727. https://doi.org/10.1016/j.celrep.2014.09.017

Richardson, C.L., L.L. Delehanty, G.C. Bullock, C.M. Rival, K.S. Tung, D.L. Kimpel, S. Gardenghi, S. Rivella, and A.N. Goldfarb. 2013. Isocitrate ameliorates anemia by suppressing the erythroid iron restriction response. *J. Clin. Invest.* 123:3614–3623. https://doi.org/10.1172/JCI68487

Rishi, G., E.S. Secondes, D.F. Wallace, and V.N. Subramaniam. 2016. Hematopoietic deletion of transferrin receptor 2 in mice leads to a block in erythroid differentiation during iron-deficient anemia. *Am. J. Hematol.* 91:812–818. https://doi.org/10.1002/ajh.24417

Rosati, A., C. Tetta, J.I. Merello, I. Palomares, R. Perez-Garcia, F. Maduell, B. Canaud, and P. Aljama Garcia. 2015. Cumulative iron dose and resistance to erythropoietin. *J. Nephrol.* 28:603–613. https://doi.org/10.1007/s40620-014-0127-3

Rozman, M., T. Masat, E. Feliu, and C. Rozman. 1992. Dyserythropoiesis in iron-deficiency anemia: ultrastructural reassessment. *Am. J. Hematol.* 41:147–150. https://doi.org/10.1002/ajh.2830410302

Singh, S., R. Verma, A. Pradeep, K. Leu, R.B. Mortensen, P.R. Young, M. Oyasu, P.J. Schatz, J.M. Green, and D.M. Wojchowski. 2012. Dynamic ligand modulation of EPO receptor pools, and dysregulation by polycythemia-associated EPOR alleles. *PLoS One.* 7:e29064. https://doi.org/10.1371/journal.pone.0029064

Sulahian, R., O. Cleaver, and L.J. Huang. 2009. Ligand-induced EpoR internalization is mediated by JAK2 and p85 and is impaired by mutations responsible for primary familial and congenital polycythemia. *Blood.* 113:5287–5297. https://doi.org/10.1182/blood-2008-09-179572

Sun, Y., M. Aiga, E. Yoshida, P.O. Humbert, and S.X. Bamji. 2009. Scribble interacts with beta-catenin to localize synaptic vesicles to synapses. *Mol. Biol. Cell.* 20:3390–3400. https://doi.org/10.1091/mbc.E08-12-1172

Sunder-Plassmann, G., and W.H. Hörl. 1995. Importance of iron supply for erythropoietin therapy. *Nephrol. Dial. Transplant.* 10:2070–2076.

Sunder-Plassmann, G., and W.H. Hörl. 1997. Erythropoietin and iron. *Clin. Nephrol.* 47:141–157.

Talbot, A.-L., G.C. Bullock, L.L. Delehanty, M. Sattler, Z.J. Zhao, and A.N. Goldfarb. 2011. Aconitase regulation of erythropoiesis correlates with a novel licensing function in erythropoietin-induced ERK signaling. *PLoS One.* 6:e23850. https://doi.org/10.1371/journal.pone.0023850

Tanimura, N., E. Miller, K. Igarashi, D. Yang, J.N. Burstyn, C.N. Dewey, and E.H. Bresnick. 2016. Mechanism governing heme synthesis reveals a GATA factor/heme circuit that controls differentiation. *EMBO Rep.* 17:249–265. https://doi.org/10.15252/embr.201541465

Tanno, T., S.-J. Noh, C. Byrnes, A. Bhupatiraju, E.R. Meier, A. Rabel, Y.T. Lee, S. Leitman, and J.L. Miller. 2008. Iron depleted erythropoiesis: slow but effective. *Blood.* 112:418.

Yamben, I.F., R.A. Rachel, S. Shatadal, N.G. Copeland, N.A. Jenkins, S. Warming, and A.E. Griep. 2013. Scrib is required for epithelial cell identity and prevents epithelial to mesenchymal transition in the mouse. *Dev. Biol.* 384:41–52. https://doi.org/10.1016/j.ydbio.2013.09.027

Yang, Z., S.B. Keel, A. Shimamura, L. Liu, A.T. Gerds, H.Y. Li, B.L. Wood, B.L. Scott, and J.L. Abkowitz. 2016. Delayed globin synthesis leads to excess heme and the macrocytic anemia of Diamond Blackfan anemia and del(5q) myelodysplastic syndrome. *Sci. Transl. Med.* 8:338ra67. https://doi.org/10.1126/scitranslmed.aaf3006

Zhao, B., Y. Mei, J. Yang, and P. Ji. 2016. Erythropoietin-regulated oxidative stress negatively affects enucleation during terminal erythropoiesis. *Exp. Hematol.* 44:975–981. https://doi.org/10.1016/j.exphem.2016.06.249